Natural Resources for Human Health
eISSN: 2583-1194

Original Research

Received 19 July 2026
Revised 22 Aug 2026
Accepted 08 Sept 2026

Natural Resources for Human Health 2026, Vol. 6 (21s):996–1025

KEYWORDS:
critical pitting temperature; electrochemical noise; bispectrum; higher-order spectral analysis; wavelet transform; pitting corrosion; passive film; stainless steel; 904L; hyper-duplex S32707; seawater; brine; localized corrosion; predictive monitoring.

Higher-Order and Time–Frequency Analysis of Electrochemical Noise for Critical Pitting Temperature Assessment of Stainless Steels in Chloride Media: A Review Linking Bispectrum and Wavelet Signatures to Localized Corrosion

Dr. Mohammed Saleh Al Ansari

Associate Professor, College of Engineering, Department of Chemical Engineering, University of Bahrain, Bahrain
Malansari.uob@gmail.com; https://orcid.org/0000-0001-9425-0294

ABSTRACT: The most important degradation mechanism for the service life of stainless steels in chloride-bearing environments such as concentrated brine systems, desalination trains and seawater cooling circuits is still localized pitting corrosion. Unlike a pitting potential measured at a single temperature, the critical pitting temperature (CPT) is the temperature threshold between self-healing and self-sustaining corrosion and is the most objective measure of an alloy's resistance to localized attack of chloride. CPT is the lowest temperature at which a metastable pit can become a stable pitting pit. In this paper, we offer a unified perspective on how an alloy approaches and crosses the CPT using electrochemical noise (EN) and its higher-order and time-frequency transformations, the bispectrum and the discrete wavelet transform. We focus on EN, power spectral density, higher order spectrum analysis, and wavelet decomposition as signal processing techniques in the first section of the review. We also give their statistical basis, sensitivity to transient events, and blind spots regarding any one corrosion parameter. In the second section, we relate all of these methods to the physical metallurgy and electrochemistry of pitting by showing why the CPT differs by tens of degrees between potentiostatic tests for sodium chloride (ASTM G150) and ferric chloride immersion (ASTM G48), as well as how the threshold is formed by passive film chemistry. The key point is that the metastable-to-stable pitting transition is nonlinear in nature, with the quadratic phase coupling as a discrete peak in the bispectrum as the wavelet energy distribution changes from fine to coarse crystals, and as the temperature increases towards the CPT, the individual passive-film rupture events stop being statistically independent and come to be the result of shared diffusion fields and local acidification. Here is the case study for hyper-duplex UNS S32707 and super-austenitic 904L. We show that EN-based temperature (58-65 °C) predictions for CPT are the same as electrochemical methods but also provide early non-perturbative warning based on potentiodynamics, potentiostatic, impedance, and electrochemical noise measurements of S32707 in sodium chloride. To provide a more data-driven model of corrosion monitoring and digital twin applications, we conclude our study by presenting a data-driven acquisition-prediction process that combines higher-order, wavelet, and statistical descriptors.

Natural Resources for Human Health
eISSN: 2583-1194

1. INTRODUCTION

Chloride-induced pitting is among the most insidious forms of corrosion because it concentrates a large amount of damage into a very small area, often propagating undetected beneath an apparently intact surface until perforation, leakage or stress-corrosion cracking suddenly compromises a component (Frankel, 1998; Szklarska-Smialowska, 1986). Stainless steels owe their corrosion resistance to a thin, chromium-enriched passive oxide film only a few nanometres thick; the durability of this film in the presence of aggressive anions ultimately decides whether a component survives for decades or fails within months (Marcus, 2011; Macdonald, 2011). In seawater, desalination brine and produced-water systems the combination of high chloride activity, elevated temperature and, frequently, oxidising biocides pushes conventional austenitic grades well beyond their safe operating envelope, which is why material selection for these duties has driven the development of increasingly highly alloyed austenitic, duplex, super-duplex and hyper-duplex stainless steels (Davis, 2000; Sedriks, 1996).

Within this context the critical pitting temperature has emerged as the parameter that engineers and corrosion scientists most often use to rank alloys and to set operating limits. The physical appeal of the CPT is that it is a threshold rather than a rate: below the CPT, pits that nucleate are unable to sustain the local chemistry required for continued growth and repassivate, whereas above it the same pits stabilise and propagate almost without limit (Laycock & Newman, 1997; Salinas-Bravo & Newman, 1994). The existence of such a sharp, reproducible threshold makes CPT far more informative for design than a single pitting potential, which is strongly dependent on the temperature and scan rate at which it happens to be measured (Frankel, 1998). Nevertheless, the way CPT is measured, and the electrolyte in which it is measured, exert an enormous influence on the reported value; a recurring source of confusion in the applied literature is the direct comparison of ferric-chloride immersion results with electrochemical results obtained in sodium chloride, which can differ by 30–50 °C for the same alloy (ASTM International, 2020; About Corrosion, 2013). Clarifying this point for stainless steels is one explicit objective of the present review.

A parallel and, until recently, largely separate line of research has developed powerful signal-analysis techniques for interrogating the spontaneous electrochemical fluctuations that accompany corrosion. Electrochemical noise—the small, unforced fluctuations of potential and current that arise from the stochastic making and breaking of the passive film—contains rich information about the type, intensity and mechanism of a corrosion process, and it can be recorded without perturbing the system (Cottis, 2001; Bertocci et al., 1997). The challenge has always been extraction: the raw noise record is a superposition of many overlapping transients, drift and instrument noise, and the diagnostic content is not obvious from casual inspection (Cottis, 2001). A succession of analysis frameworks has therefore been imported from statistical signal processing—time-domain statistics, power spectral density estimation, higher-order (polyspectral) analysis and, more recently, wavelet and other time–frequency transforms—each contributing a different view of the same underlying events (Aballe et al., 2001; Suresh & Kamachi Mudali, 2014; Darowicki & Zieliński, 2008). Two of these frameworks are of particular interest for pitting and are the analytical focus of this review: higher-order spectral analysis, epitomised by the bispectrum, and time–frequency analysis, epitomised by the discrete wavelet transform. The bispectrum is sensitive to nonlinear phase coupling between frequency components and therefore to the departure of a signal from Gaussian, linear behaviour; the wavelet transform localises transient energy simultaneously in time and in scale and therefore resolves the birth, growth and death of individual pitting events (Nikias & Petropulu, 1993; Aballe et al., 1999).

The core proposition explored here is that the metastable-to-stable pitting transition that defines the CPT is precisely the kind of physical process these two methods are built to detect: as an alloy is heated toward its CPT, discrete passive-film rupture events become more frequent, longer-lived and—crucially—mutually correlated, so that the statistics of the noise record change in ways that are far more clearly expressed in the bispectrum and the wavelet energy distribution than in the mean current or the noise resistance alone (Darowicki & Zieliński, 2008; Suresh & Kamachi Mudali, 2014). The review is organized to be able to get to this point slowly. In order to understand the mathematical features, advantages and disadvantages of electrochemical noise, power spectral density, bispectrum and wavelet transform on their own terms before applying them, Section 2 is a self-contained literature review of the signal analysis techniques and specifically, the CPT. CPT for stainless steels is defined in detail in Section 3 and the reasons why measured values differ so much between techniques and how metallurgy and passive film chemistry control the threshold are explained. The CPT of the main commercial alloy families is compared in Section 4 and a detailed case study of hyper-duplex S32707 in sodium chloride and 904L in saltwater and brine is provided in Section 5. This is also carried out for wavelet and integrated

time-frequency signatures in Section 6 and for an optimal, integrated method to estimate CPT and provide early warning of localized corrosion is proposed in Section 7. In Section 8, we draw conclusions and discuss some unresolved issues. Considering this, we consider four aspects in this review.

To assist the reader in reconciling the many different values quoted in the literature, we first present in one place a specific description of the critical pitting temperature for stainless steels, and we treat the method-and electrolyte-dependence of the value as the key issue rather than a footnote. Second, we discuss the relevant signal-analysis techniques as generic instruments, in the absence of corrosion, and we find that they are in good order of validity in order to apply. Third, based on the bispectral results of Darowicki and Zieliński (2008), the wavelet results of Suresh and Kamachi Mudali (2014) and the multi-method CPT validation of Xu et al. (2018), it describes in physical terms the mechanistic connection between the nonlinear pit-interaction process which defines the CPT and the higher order and time-frequency signatures that electrochemical noise carries. Fourth, it draws the lines between the state of the art and a deployed, predictive corrosion management tool and synthesizes these studies into a coherent approach. This review is restricted to chloride-induced pitting of stainless steels and does not attempt to address microbiologically driven corrosion, stress corrosion or crevice corrosion.

2. A SYSTEMATIC ASSESSMENT OF CORROSION SIGNAL ANALYSIS TECHNIQUES

We review the family of signal analysis techniques to be used to solve the pitting problem in this section. Each method is considered as a general tool to collect information from an electrochemical signal that changes. The purpose of this discussion is to identify from a mathematical and statistical perspective what each approach is monitoring, what assumptions are made, and where it fails in the process; we do not include the critical pitting temperature or any other corrosion parameter. The approaches can only be rationally matched to the physical events they are expected to detect once these features are evident.

2.1 Electrochemical Noise: Physical Origin And Measurement

Electrochemical noise (EN) is the low-level fluctuations of electrode potential (e.g., in the absence of external interference) and current between two or more electrodes. Nucleation and repair of local defects in a surface film, the discrete detachment of gas bubbles, adsorption and desorption of ions, and localized dissolution transients are the most basic stochastic processes of the electrochemical interface, and they contribute to these fluctuations (Cottis, 2001; Bertocci et al., 1997). Unlike polarization techniques, which impose a potential or current that in turn transforms the surface state, EN has the advantage of not affecting the processes it seeks to study because the measurement is passive (Bertocci et al., 1997).

The potential noise between the working electrode and a reference and current noise between two (nominally identical) working electrodes are recorded in the laboratory in a normal laboratory setting with a zero-resistance ammeter, and the potential scale is set by a third reference electrode (Cottis, 2001). These are two practical problems that limit the quality of the data. The first is instrumental: the sampling rate and record length must be chosen so that the transients of interest are detected without aliasing, and the amplifier and zero-resistance ammeter must be less noisy than corrosion (Bertocci et al., 1997). The second is to eliminate direct current drift. The low-frequency end of any subsequent spectral estimate is infected with the slow wandering of the mean potential or current due to slow changes in the surface area or open-circuit potential. This drift needs to be removed by detrending, by polynomial subtraction, by moving average filtering, or in the most recent work by wavelet-based removal of the smooth part of the signal (Tan et al., 1996; Aballe et al., 1999). The choice of detrending technique is not neutral: under-detrending will leave drift that appears to be a corrosion signal, while over-detrending will remove real low-frequency information.

A few quantities are immediately relevant from the coupled potential and current records. Increasing R_n means more corrosion. The noise resistance, R_n, is the ratio between the standard deviation of potential and the standard deviation of current. It has the units of resistance as well and for many systems correlates broadly with polarization resistance (Cottis, 2001). The spectral noise resistance extends the idea to the frequency domain. These amounts are attractive because they are easy to obtain, but they will remove nearly all the information about the timing and structure of individual events (which the techniques we will describe below are attempting to recover) by reducing

the whole record to one or two numbers. Shot-noise theory, which views the current record as a superposition of elementary charge-transfer events in the form of a packet of charge that is transferred to the external circuit, is more physically applicable for electrochemical noise (Sánchez-Amaya et al., 2005; Cottis, 2001).

Within this framework two quantities can be extracted that have direct mechanistic meaning: the characteristic charge carried by a single event, obtained from the ratio of the current power spectral density to the mean current, and the frequency of events, obtained from the mean current and the characteristic charge together. A process dominated by a few large events—localized corrosion—yields a large characteristic charge and a low event frequency, whereas uniform corrosion yields the opposite; the shot-noise parameters therefore discriminate corrosion mechanisms on a firmer basis than the empirical localization index (Sánchez-Amaya et al., 2005). The value of this view for the present review is conceptual: it makes explicit that an electrochemical-noise record is a point process of discrete events, and it is the changing statistics of that point process—the growth in event charge, the change in event rate and, above all, the emergence of correlation between events—that the higher-order and time–frequency methods are ultimately quantifying.

2.2 Time-Domain Statistical Descriptors

The most direct interrogation of an EN record is statistical. After detrending, the potential and current series can be summarised by their moments and by descriptors derived from them. The variance measures the overall energy of the fluctuations; the skewness measures the asymmetry of the amplitude distribution, distinguishing records dominated by sharp one-sided transients from symmetric noise; and the kurtosis measures the 'peakedness' of the distribution and is elevated when a record contains rare, large excursions against an otherwise quiet background (Cottis, 2001; Sanchez-Amaya et al., 2005). Discrete non-Gaussian events are identified statistically by deviation from the zero skewness and three kurtosis of a Gaussian process. In corrosion, two composite characteristics are now considered standard. In order to distinguish between uniform corrosion which results in numerous small overlapping events with a low index and localized corrosion which results in a few large discrete events with an index that is close to 1, the localization index, which is defined as the ratio of the current's standard deviation to its root mean square value, is in the range of 0 to 1 (Cottis, 2001). The localization index is still a common first pass diagnostic but is criticized by some as it is sensitive to the electrode area and measurement configuration (Cottis, 2001; Sanchez-Amaya et al., 2005). Transient counting methods are a more explicit and data-driven method that identify and record each current or potential excursion and then statistics of its amplitude, rise time and decay time. The shape of a transient carries mechanistic information because decay represents the arrest or repair of an event, whereas rise reflects its nucleation and growth (Pistorius & Burstein, 1992; Aballe et al., 1999). The limitation of all purely time-domain statistics is that they treat the record as a bag of amplitudes and largely ignore how the events are distributed in frequency, in scale and in their coupling to one another.

2.3 Frequency-Domain Analysis: Power Spectral Density

The power spectral density (PSD) describes how the variance of a signal is distributed across frequency, and it is obtained either by the fast Fourier transform of the record, usually after windowing to control spectral leakage, or by parametric methods such as the maximum-entropy method (Bertocci et al., 1997; Pujar et al., 2011). For many corroding systems the current PSD exhibits a low-frequency plateau followed by a roll-off region in which the spectral power decreases with frequency according to a characteristic slope. Three parameters are commonly extracted: the plateau level, which scales with the intensity of the fluctuations; the roll-off, or corner, frequency, which marks the transition; and the roll-off slope of the high-frequency region, which has been related to the nature of the dominant transients (Bertocci et al., 1997; U.S. Patent 5,888,374).

The roll-off slope has proven diagnostically valuable because processes dominated by a few slow, large-amplitude transients produce steeper slopes than processes dominated by many fast, small events (Bertocci et al., 1997). However, the PSD carries an inherent and often overlooked limitation: it retains only the magnitude of each frequency component and discards the phase. Two records with identical power spectra can have completely different temporal structure, because all information about when events occur and about how frequency components are phase-related is contained in the phase that the PSD throws away (Nikias & Petropulu, 1993). For a signal composed of independent, randomly timed transients this loss is unimportant, but for a signal in which events are correlated it is fatal: the PSD is, by construction, blind to the very inter-event coupling that

distinguishes an organised process from a random one. Higher-order spectrum analysis was specifically designed to deal with this problem.

The trade-off between parametric and non-parametric methods is also an important dimension to consider in spectral estimation. While parametric methods like autoregressive or maximum entropy modeling can produce sharper spectra from shorter records, they are still governed by a model whose order must be chosen and can lead to spurious peaks if it is not specified, the periodogram and its windowed averaged versions do not make any assumptions about the signal and need long records to provide low variance and good frequency resolution at once (Bertocci et al., 1997; Pujar et al., 2011). Both approaches are used for corrosion noise, where recordings may be shorter than the slowest processes of interest and the objective is often to follow a slow roll-off rather than to get very fine spectral detail resolution. The broader lesson, which recurs for every transform in this review, is that the spectrum is not a property of the signal alone but of the signal together with the estimation procedure, so that comparisons are meaningful only when the procedure is held fixed. This dependence is more acute still for the higher-order estimates considered next, whose variance is intrinsically larger than that of the second-order spectrum (Nikias & Petropulu, 1993).

2.4 Higher-Order Spectral Analysis And The Bispectrum

Higher-order spectra, or polyspectra, generalise the power spectrum by using higher-order moments and cumulants of a signal rather than the second-order autocorrelation on which the PSD is based (Nikias & Petropulu, 1993). The bispectrum, the simplest higher-order spectrum, is the double Fourier transform of the third-order cumulant of a signal and is a function of two frequencies, f_1 and f_2. Its magnitude at a point (f_1, f_2) measures the degree of quadratic phase coupling among the three frequency components f_1, f_2 and their sum f_1+f_2 (Nikias & Petropulu, 1993; Collis et al., 1998). Two properties make the bispectrum uniquely suited to detecting organised, nonlinear behaviour. First, for a Gaussian process the third-order cumulant—and therefore the bispectrum—is identically zero; a non-zero bispectrum is direct evidence that the signal is non-Gaussian. Second, for a linear process with statistically independent frequency components the bispectrum also vanishes; a non-zero bispectrum therefore additionally indicates nonlinearity and phase coupling between components (Nikias & Petropulu, 1993).

The bispectrum locates such interactions precisely in the bifrequency plane, producing discrete peaks whose position identifies the coupled frequencies and whose height measures the strength of coupling (Collis et al., 1998). A normalised version, the bicoherence, rescales the bispectrum by the power at the participating frequencies so that it varies between zero and one and can be interpreted as the fraction of power at the sum frequency that is phase-coupled to the lower frequencies; the bicoherence is preferred when the aim is to compare coupling strength across records of different overall energy (Collis et al., 1998; Nikias & Petropulu, 1993).

Because the third-order cumulant preserves information about the occurrence time and time constant of transients that the power spectrum destroys, the bispectrum and its integrated forms have been proposed as sensitive detectors of transient, non-Gaussian events in noisy records (Darowicki & Zieliński, 2008). Higher-order spectral analysis has a longer history in fields such as acoustics, mechanical vibration and biomedical signal processing, where it is used to detect the onset of nonlinear coupling that heralds a change of regime—turbulence, gear-tooth damage or physiological transition (Nikias & Petropulu, 1993; Collis et al., 1998). The same reasoning behind its more recent application to electrochemical signals: a corroding surface that has begun to organize itself into interacting, self-reinforcing events would produce phase-coupled fluctuations that appear in the bispectrum long before they dominate the mean current.

The main practical drawbacks of higher-order analysis are its processing cost in comparison with the PSD and its thirst for data (long, well-conditioned records are necessary to accurately estimate a two-dimensional cumulant) (Nikias & Petropulu, 1993). It is necessary to make a practical comment on estimation since it influences everything that comes after. The indirect method, which computes the third-order cumulant sequence and then Fourier-transforms it, and the direct method, which creates triple products of the Fourier coefficients of overlapping data segments and averages them, are two generally equivalent methods for estimating the bispectrum (Nikias & Petropulu, 1993).Both require averaging over many segments to suppress the large variance of the raw estimate, and both trade resolution in the bifrequency plane against variance; the choice of segment length, overlap and window therefore materially affects the appearance of the bispectrum surface. Symmetry properties of the bispectrum mean that it is fully determined by a

triangular region of the bifrequency plane, which reduces computation, but the fundamental appetite for data remains (Collis et al., 1998). These considerations explain why higher-order analysis was slower than spectral analysis to enter routine corrosion practice: only with modern acquisition and computing has it become straightforward to record and process the long, well-sampled records that reliable bispectral estimation demands. They also foreshadow the methodological cautions of Section 5.6, where the same estimation choices are shown to affect the reliability of a bispectral CPT criterion.

2.5 Wavelet And Time–Frequency Analysis

Fourier-based approaches like bispectrum explain the frequency content of a record but not its time evolution - the statistical properties of the signal are assumed to remain constant during the analysis window. Time-frequency techniques that determine when and at what scale energy occurs are very interesting because corrosion records are often non-stationary (the nature of the fluctuations changes as the surface changes) (Aballe et al., 1999; Homborg et al., 2012). One such approach is to use a short-time Fourier transform, but it is limited by a set window and hence by a fixed, uniform resolution in time and frequency. By correlating the signal with scaled and translated copies of a compact analyzing function, the wavelet transform breaks this restriction and provides a fine time resolution at high frequencies and a fine frequency resolution at low frequencies.

In corrosion practice the discrete wavelet transform is applied through a multiresolution decomposition that successively splits the record into detail coefficients at a sequence of dyadic scales, conventionally labelled D1, D2, …, D8, together with a residual smooth component S8 (Aballe et al., 1999; Suresh & Kamachi Mudali, 2014). The relative energy contained in each scale, plotted as the energy distribution plot (EDP), summarises which timescales dominate the record. A widely used physical mapping associates the finest crystals (roughly D1–D3) with rapid, short-lived events, the intermediate crystals (D4–D6) with localized processes of intermediate duration, and the coarsest crystals (D7–D8) with slow, diffusion-controlled processes, while S8 captures residual direct-current content (Aballe et al., 1999; Cardenas-Barrera et al., 2024). A complementary construction, the standard-deviation-of-partial-signals plot, tracks the standard deviation reconstructed from each scale and has been recommended alongside the EDP because it responds to the frequency of the predominant transients and hence, indirectly, to event density (Shahidi et al., 2011).

The strength of wavelet analysis is that it preserves temporal localisation while still resolving scale, so it can follow the migration of energy between timescales as a process evolves and can flag the exact moment at which a new class of event appears (Aballe et al., 1999; Homborg et al., 2012). Its principal weakness is a degree of arbitrariness: the results depend on the choice of analysing wavelet and on the depth of decomposition, and the mapping between crystals and physical processes, though useful, is empirical rather than exact (Shahidi et al., 2011). Similar time-frequency techniques like the Hilbert-Huang transform based on empirical mode decomposition and recurrence plot analysis have shown promising utility in corrosion signals and are employed to address non-stationarity in a variety of situations, particularly when the record is short or the fluctuations are very non-linear (Homborg et al., 2012; Hou et al., 2017).

The application of wavelet analysis in corrosion analysis is shaped by two important practical factors. First, a smoother family, like symlets or coiflets, can be preferred when the goal is to reconstruct the underlying trend rather than transient data. The second is that the same multiresolution setup that is used in the analysis is also a denoising and detrending tool. The slow direct current drift can be eliminated without having to deal with the phase distortion due to polynomial fitting by discarding or thresholding the coefficients of the coarsest smooth component, and the mid-scale corrosion transients can be captured while the instrumental white noise is suppressed by thresholding the finest details (Aballe et al., 1999; Homborg et al., 2012). Considering their dual role, wavelet analysis is often the first and the last step in the process of analyzing an electrochemical noise record. Care should be taken to ensure that the decision to pre-process does not conflict with the conclusions that are drawn from the energy distribution.

Also, one should distinguish between the discrete wavelet transform which is computationally cheaper and samples scale and translation on a dyadic grid and the continuous wavelet transform that evaluates the transform on a fine grid of scales and generates a redundant but visually informative scalogram. For quantitative energy accounting the discrete transform is preferred because its orthogonality guarantees that the energies of the crystals sum to the total energy of the record; for the visual identification of when a particular class of transient appears, the continuous transform and its

associated ridges can be more revealing (Homborg et al., 2012). In either form, the essential value of the method for the present purpose is that it converts a one-dimensional record into a two-dimensional time–scale representation in which the appearance and growth of a new population of events becomes directly visible, a capability that neither the power spectrum nor the bispectrum, both of which integrate over time, can provide on its own.

2.6 Data-Driven And Machine-Learning Interpretation

The parameters produced by the preceding methods—statistical moments, roll-off slopes, bispectral peak intensity and entropy, wavelet crystal energies—constitute a feature vector that describes the state of a corroding surface at a given time. A natural development, accelerated by advances in machine learning, has been to feed these features to classification and regression models rather than to interpret them one at a time (Hou et al., 2017; Cardenas-Barrera et al., 2024). Supervised classifiers—support-vector machines, random forests, linear discriminant analysis and neural networks—have been trained to distinguish corrosion types and stages from EN-derived features, while unsupervised methods have been used to detect changes of regime without labelled data (Hou et al., 2017; Calabrese et al., 2023). Recurrence quantification analysis, which measures the determinism and predictability of a time series, has been combined with machine learning to interpret EN records and found to complement the frequency-domain descriptors (Hou et al., 2017).

Two cautions temper enthusiasm for the data-driven route. First, a model is only as trustworthy as its training set: features extracted from one alloy, electrolyte and cell geometry do not necessarily transfer to another, and the physical meaning of a learned decision boundary can be opaque (Cardenas-Barrera et al., 2024). Second, the quality of the features still depends on the signal-processing choices reviewed above, so a machine-learning layer does not remove the need to understand the underlying transforms—it inherits their strengths and their blind spots. The most promising recent work therefore fuses complementary descriptors, deliberately combining a higher-order feature such as bispectral entropy, which is sensitive to nonlinear coupling, with a wavelet feature such as the energy distribution, which is sensitive to timescale, so that the model receives information no single transform could supply (Calabrese et al., 2023; Cardenas-Barrera et al., 2024).

A distinction is emerging within the data-driven literature between feature-based models, which operate on the hand-crafted descriptors described above, and end-to-end models, which attempt to learn directly from the raw or lightly conditioned noise record using convolutional or recurrent neural architectures (Calabrese et al., 2023; Cardenas-Barrera et al., 2024). Feature-based models have the advantage of interpretability, because each input descriptor has a known physical meaning, and of modest data requirements, since the domain knowledge encoded in the transforms does much of the work; they are well suited to the CPT problem, where the number of labelled temperature ramps available for training is inevitably limited. End-to-end models can in principle discover discriminating structure that the pre-defined descriptors miss, but they demand far larger datasets and sacrifice transparency, which is a serious drawback in a safety-related engineering context where the basis of a prediction must be defensible.

For the foreseeable future the pragmatic choice for CPT assessment is a feature-based model built on the physically motivated bispectral, wavelet and statistical descriptors of this review, with the transforms serving as an informed, interpretable form of dimensionality reduction that keeps the model anchored to the mechanism (Calabrese et al., 2023; Cardenas-Barrera et al., 2024).

2.7 Synthesis: Complementary Rather Than Competing Methods

The methods reviewed above are best understood as complementary lenses on the same fluctuating signal. Time-domain statistics answer how large and how asymmetric the fluctuations are; the power spectrum answers how their energy is distributed across frequency but discards phase; the bispectrum recovers the phase relationships and so answers whether the events are nonlinearly coupled; and the wavelet transform answers when, and at what timescale, events occur. Table 1 summarises these roles. A recurring theme of the applied literature is that no single method is sufficient: the most robust interpretations come from combining a phase-sensitive higher-order descriptor with a time-localised wavelet descriptor and grounding both in the physical picture of the process being studied (Suresh & Kamachi Mudali, 2014; Darowicki & Zieliński, 2008; Cardenas-Barrera et al., 2024). It is this combination that the remainder of the review brings to bear on the pitting of stainless steels and, specifically, on the detection of the critical pitting temperature.

Table 1. Complementary signal-analysis methods for electrochemical noise, their primary output and their intrinsic limitation.

Method	Domain	What it measures	Key descriptor(s)	Intrinsic limitation
Statistical moments	Time	Amplitude and shape of fluctuations	Variance, skewness, kurtosis, localization index	Ignores timing and frequency coupling
Transient counting	Time	Individual event shape and rate	Amplitude, rise/decay time, event density	Sensitive to overlap and thresholding
Power spectral density	Frequency	Energy vs. frequency	Plateau, corner frequency, roll-off slope	Discards phase; blind to coupling
Bispectrum / bicoherence	Higher-order frequency	Quadratic phase coupling; non-Gaussianity	Bispectral peak, energy, entropy; bicoherence	Data-hungry; computationally heavy
Wavelet transform (DWT)	Time–frequency	Energy vs. timescale, localised in time	Crystal energies D1–D8/S8; EDP; SDPS	Depends on wavelet choice; empirical mapping
Machine learning	Feature space	Classification / regression of state	Learned decision boundaries	Needs training data; can be opaque

DWT = discrete wavelet transform; EDP = energy distribution plot; SDPS = standard deviation of partial signals.

Source: compiled by the authors.

2.8 Signal Conditioning And The Risk Of Pre-Processing Artefacts

A methodological review of these tools would be incomplete without a word on the conditioning that precedes every analysis, because the descriptors that follow are only as trustworthy as the signal conditioning that produces them. Raw electrochemical-noise records contain, in addition to the corrosion signal of interest, instrumental noise, mains interference, quantisation effects and the slow direct-current drift already discussed; each of these can masquerade as, or obscure, genuine corrosion structure if not handled correctly (Bertocci et al., 1997; Cottis, 2001). The most important phase is drift reduction. Moving average and high-pass filtering shift and attenuate the very transients of interest; polynomial detrending is straightforward but imposes its own low-frequency structure and can distort the phase relationships on which the bispectrum depends; and wavelet-based removal of the smooth component, although cleaner in theory, still depends on the choice of decomposition depth (Aballe et al., 1999; Homborg et al., 2012).

The practical rule that emerges from the literature is that conditioning choices must be reported and held constant within any comparison, because a change in detrending or windowing can shift a descriptor by more than the effect being studied. This is especially important for the higher-order and time–frequency descriptors that are the focus of this review, since both are sensitive to phase and to low-frequency content. Sampling rate and record length must likewise be matched to the phenomenon: too low a rate aliases fast transients into the analysis band, while too short a record starves the bispectral estimate of the averaging it needs (Nikias & Petropulu, 1993). None of these considerations is unique to corrosion, but their neglect is a common reason that nominally similar studies report divergent descriptor values, and their standardisation is a precondition for the cross-laboratory comparability that a signal-based CPT criterion would require.

3. CRITICAL PITTING TEMPERATURE OF STAINLESS STEELS: A CLARIFIED ACCOUNT

Having established the analytical tools in isolation, we now turn to the physical parameter they will be used to detect. This section sets out, as clearly as the evidence allows, what the critical pitting temperature is for stainless steels, the mechanism that gives rise to it, and—most importantly for readers trying to reconcile conflicting numbers in the literature—why measured CPT values depend so strongly on the test method and electrolyte.

3.1 Physical Meaning And Definition

The lowest temperature at which stable pitting corrosion on a given alloy is started and maintained under a particular combination of electrochemical and environmental conditions is known as the critical pitting temperature (Salinas-Bravo & Newman, 1994; Laycock & Newman, 1997). "Stable" is a very important concept. A passive stainless steel surface in chloride solution is constantly nucleating small metastable pits at any temperature from ambient; most of these pits repassivate in milliseconds to seconds and do not cause long-term damage (Pistorius & Burstein, 1992; Frankel, 1998). A growing number of these pits are becoming self-sustaining and can survive indefinitely at and above the CPT, which is the temperature at which the balance tips. Almost all nucleated pits repassivate below this temperature (Laycock & Newman, 1997). The CPT behaves like a material property in contrast to the pitting potential that is constantly and strongly variable with temperature, because this transition is sharp and repeatable for a well-prepared surface. This reproducibility is what makes the CPT valuable in engineering (Frankel, 1998; ASTM International, 2020).

3.2 Mechanistic Basis: The Metastable-To-Stable Transition

The local chemistry in a growing pit provides the best insight into the mechanism underlying the CPT. The interior of the pit becomes acidic when the passive film ruptures locally because the exposed metal dissolves quickly and the metal cations generated hydrolyze to produce hydrogen ions. At the same time, chloride ions migrate into the pit to maintain charge neutrality, significantly increasing the local chloride concentration far above that of the bulk (Galvele, 1976; Frankel, 1998). The hostile local environment with high chloride and low pH maintains dissolution by preventing the passive film from regenerating. A struggle between the rate at which this hostile chemistry is produced by dissolution and the rate at which it is dispersed by diffusion out of the pit determines whether a pit survives (Galvele, 1976; Laycock & Newman, 1997).

The dynamics of this rivalry depend on temperature. While the diffusive dissipation that would heal the pit is only slightly affected by temperature, the anodic dissolution kinetics which produce the aggressive chemistry are thermally activated and accelerate strongly (Laycock & Newman, 1997; Salinas-Bravo & Newman, 1994). Above the CPT, generation is the dominant process and a very important local chemistry is preserved, so that the pits stabilize; below the CPT, dissipation is all but the most significant transients and the pits repassivate. Such a strong nonlinear temperature dependency of the dissolution kinetics and the salt-film stability that leads to high dissolution rate is reflected in the rather sharp threshold (Laycock & Newman, 1997). This mechanistic scenario also has a crucial corollary that keeps coming up in this review: close to the CPT, the survival of one pit changes the local chemistry of its neighbors. This is the physical basis for the nonlinear coupling that higher order signal analysis is meant to identify.

Galvele (1976) introduced the pit-stability criterion, which makes the competition quantitative. He showed that the survival of the aggressive local chemistry inside a pit depends on the product of the pit depth and the local current density exceeding a critical value; below which the acidified, chloride-rich electrolyte is diluted by diffusion faster than dissolution can regenerate it and the pit repassivates (Galvele, 1976; Frankel, 1998). The strong thermal activation of the anodic dissolution current allows temperature to enter this criterion. As temperature increases, the current density of the given potential increases and the critical product is reached at smaller pit depths and a higher percentage of nucleated pits pass the stability value (Laycock & Newman, 1997).

For the metastable pits that the surface creates, the CPT can be regarded as the temperature at which the pit-stability product is first able to be reached consistently. This quantitative explanation confirms the qualitative explanation provided above but also explains why the transition is so abrupt: the fraction of pits that reach stability is very high over a small temperature range due to the steep and nonlinear increase in dissolution current with temperature, which gives the CPT its character as a threshold rather than a gradual trend (Galvele, 1976; Laycock & Newman, 1997).

Natural Resources for Human Health
eISSN: 2583-1194

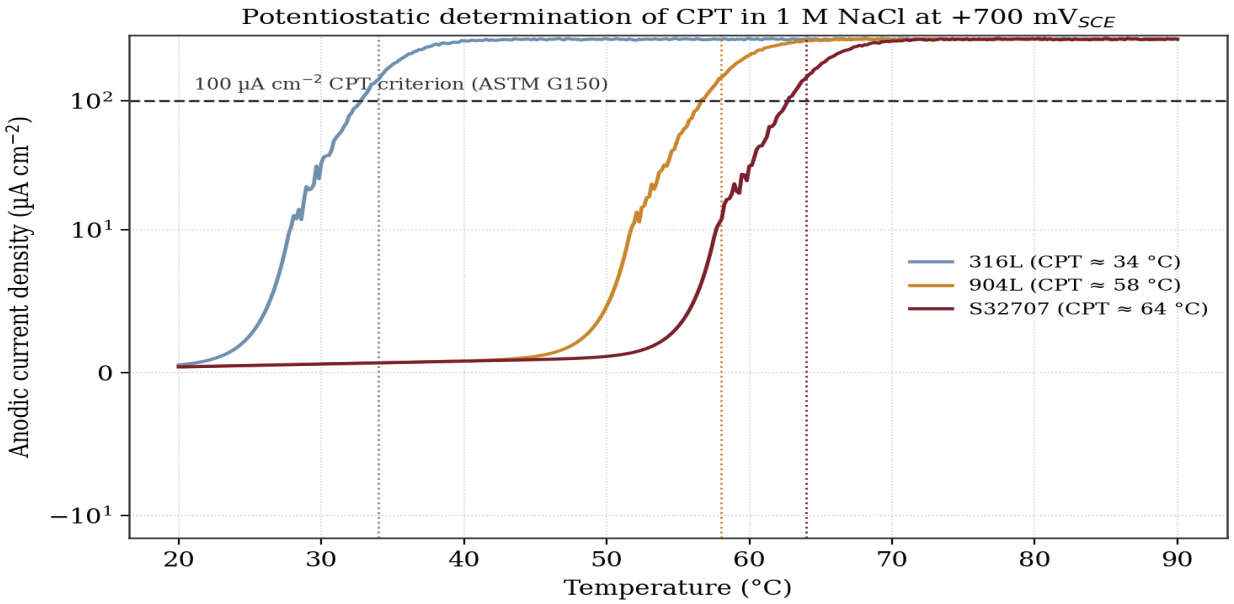

Graph 1. Potentiostatic determination of CPT

Graph 1 displays idealized potentiostatic determination of the critical pitting temperature. The specimen is held at a fixed anodic potential in sodium chloride while the temperature is ramped; the anodic current density remains at the low passive level until, at the CPT, stable pitting causes it to rise steeply and irreversibly through the 100 µA cm⁻² criterion of ASTM G150. The temperature at which the current crosses the criterion defines the measured CPT; higher-alloyed grades cross at higher temperatures. Source: schematic prepared by the authors following the ASTM G150 potentiostatic method (ASTM International, 2020).

3.3 Measurement Methods And Why Reported Values Differ

A great deal of confusion in the applied literature stems from comparing CPT values obtained by fundamentally different methods as though they were interchangeable. They are not. The two families of standardised methods measure related but distinct things in different electrolytes, and the numbers they produce for the same alloy can differ by tens of degrees.

The ferric-chloride immersion method (ASTM G48, Methods A and E) exposes specimens, with or without artificial crevices, to a strongly oxidising and highly acidic 6 % ferric chloride solution; the temperature is raised in steps until visible pitting occurs, and the lowest temperature producing attack is reported as the CPT (ASTM International, 2020). Because of the ferric ions' high oxidizing power and the acidity of the solution, this medium is deliberately more hostile than the natural chloride water (About Corrosion, 2013). The CPT for ferric chloride is conservative as usually much lower than for the same alloy that would pit by the same temperature in seawater and should be used to rank alloys and reveal metallurgical defects like sensitization or intermetallic precipitation, rather than to predict the service temperature. The potentiostatic electrochemical method (ASTM G150) keeps the specimen at a fixed anodic potential of +700 mV in a sodium chloride solution (1 M) but increases the temperature slowly. The CPT is set at which the anodic current density is more than 100 µA cm⁻² which means that the pit is stable (ASTM International standard G150; Arnvig & Bisgard, 2018).

Since the electrolyte is less aggressive than ferric chloride and the potential is stable, the G150 readings are generally larger and more physically coherent, and the process has a clear objective end. Potentiodynamic and cyclic polarization at different temperatures, temperature-scanned impedance spectroscopy, and electrochemical-noise monitoring determine the CPT at which stable pitting is first found, and these tend to be very close with the potentiostatic value in the same electrolyte (Xu et al., 2018). Readers of CPT data should always have the electrolyte and technique and the values. Figure 2 shows the point for three examples of alloys: ferric-chloride and sodium-chloride electrochemical results for the same material can vary by 30 °C or more, and the difference between the

two electrochemical methods for sodium chloride is small. Table 2 shows standard procedures. Misreading a conservative value for ferric chloride as a service limit creates expensive material selection, and misinterpreting an optimistic value for seawater as a universal value risks under-specification (About Corrosion, 2013).

A realistic improvement of electrochemical determination would make the values we have considered here very reliable. Early potentiostatic CPT experiments were sometimes hampered by specimen holder crevice corrosion, which attacked the artificial crevice far below the pitting temperature and produced spuriously low CPT results.The introduction of the Avesta cell, which flushes the specimen-holder interface with distilled water to suppress crevice initiation, largely eliminated this artefact and made the potentiostatic CPT the reproducible quantity on which ASTM G150 is based (Arnvig & Bisgard, 1996; ASTM International, 2020). The episode is instructive: it shows that even a well-defined electrochemical method can be corrupted by an experimental detail, and it underlines why the standardisation of test geometry and procedure is as important as the choice of electrolyte. It also reinforces the argument for methods, such as electrochemical noise on a crevice-free specimen, that avoid imposing artificial crevices altogether, and it is one reason the close agreement among the four crevice-sensitive and crevice-insensitive methods reported by Xu et al. (2018) for S32707 is reassuring rather than merely convenient.

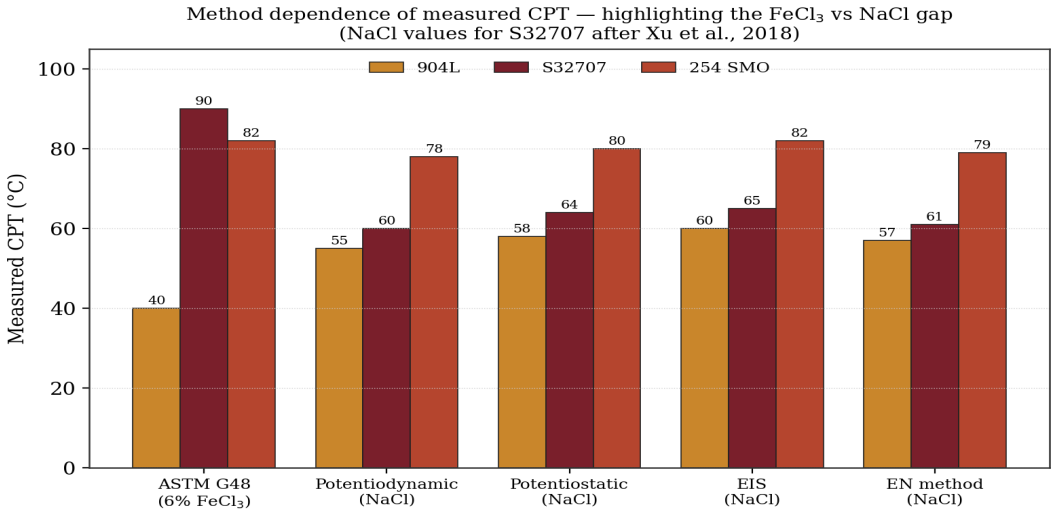

Graph 2. Method dependance of measured CPT

Graph 2 shows the method dependence of the measured critical pitting temperature for 904L, hyper-duplex S32707 and super-austenitic 254 SMO. The ferric-chloride (ASTM G48) values differ markedly from the electrochemical values obtained in sodium chloride; the sodium-chloride values for S32707 are those reported by Xu et al. (2018) using potentiodynamic, potentiostatic, impedance and electrochemical-noise methods. The figure emphasises that a CPT value is meaningful only when its test method and electrolyte are specified. Source: prepared by the authors from data reported by Xu et al. (2018) and ASTM International (2020).

Table 2. Comparison of the principal standardised methods for determining the critical pitting temperature of stainless steels. Source: compiled by the authors from ASTM International (2020), Sedriks (1996) and Davis (2000).

Attribute	**ASTM G48 (A/E)**	**ASTM G150**	**Electrochemical (PD / EIS / EN, NaCl)**
Electrolyte	6 % $FeCl_3$ (acidic, oxidising)	~1 M NaCl	0.5–3.5 % / 1 M NaCl
Principle	Stepwise immersion; visible attack	Fixed potential; current threshold	Signature of stable pitting vs. temperature

Endpoint	Lowest T giving visible pits/mass loss	$i > 100\ \mu A\ cm^{-2}$ sustained	Current jump / impedance drop / noise onset
Typical value	Conservative (low)	Higher, physically interpretable	Cluster near G150 value
Best used for	Ranking; detecting defects/heat-treatment	Design-relevant threshold	Mechanistic study; non-perturbative monitoring
Limitation	Not a service temperature	Potential must be chosen sensibly	Requires signal analysis; less standardised

PD = potentiodynamic; EIS = electrochemical impedance spectroscopy; EN = electrochemical noise.

3.4 Metallurgical And Environmental Factors Governing CPT

Beyond the test method, the CPT of a given alloy is set by its passive-film chemistry, which in turn depends on composition and microstructure. Chromium is the basis of passivity, forming the protective oxide; molybdenum is the single most effective element for raising the CPT because it stabilises the film and, more importantly, suppresses active dissolution and promotes repassivation within incipient pits; nitrogen raises the CPT by buffering the local acidification and by enriching the passive film (Newman, 2001; Marcus & Maurice, 2017). Copper and tungsten have both a few advantages in some cases (Davis, 2000). The pitting resistance equivalent number (PREN), which is usually % Cr + 3.3×%Mo + 16×%N, is one index that is correlated with CPT and is used for first-pass screening (Davis, 2000; Sedriks, 1996). The composition can be altered by microstructure and product manufacture. Pits are often initiated by non-metallic inclusions, especially manganese sulfides leading to low CPT values in bulk chemistry (Ryan et al., 2002; Frankel, 1998). If the ferrite-austenite ratio is not balanced or sigma phase, chromium nitrides, or secondary austenite is precipitated during welding or under heat treatment it will leave chromium and molybdenum locally and in a significant way pitting resistance is lost in duplex and super-duplex grades. This defect is also evident in ferric chloride testing. This is because the CPT is influenced by environmental factors like chloride concentration, oxidizing species, pH and velocity. This is why the real seawater or brine service value might be different from laboratory value (Salinas-Bravo & Newman, 1994).

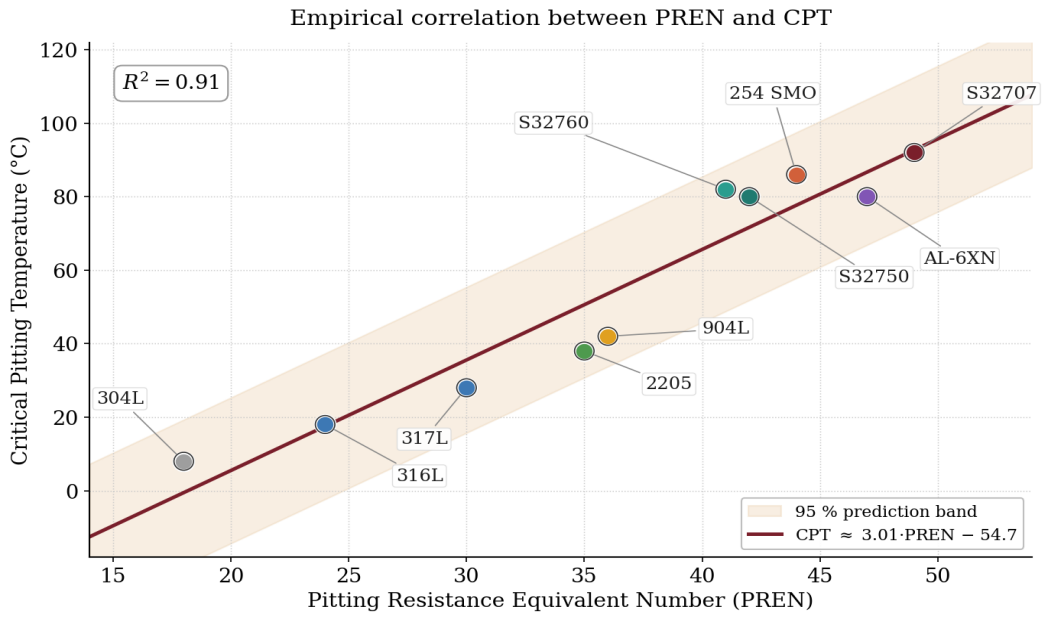

Graph 3. Empirical correlation between PREN and CPT

Graph 3 displays the pitting resistance equivalent number and critical pitting temperature of commercial stainless-steel families are correlated. The positive trend is very strong, which also supports PREN as a first-pass screening

index, while the scatter around the regression line indicates the additional microstructure, inclusions, surface polish and production that PREN cannot capture. Source: Authors' compilation of CPT and PREN data from Sedriks (1996), Davis (2000), and Xu et al. (2018).

Modern inclusion engineering—reducing the sulphur content of the steel and controlling the composition of the residual oxide and sulphide inclusions so that they are less electrochemically active—has been one of the most effective routes to improved pitting resistance in commercial practice, and it explains part of the improvement in CPT achieved by clean, modern melts relative to older heats of nominally the same grade (Ryan et al., 2002; Sedriks, 1996). The practical implication is that the CPT of a component is not fixed by its grade designation alone but by the combination of composition, melt cleanliness, heat treatment and surface finish; two specimens of the same nominal alloy can differ measurably in CPT, which is a further reason that reported values must be accompanied by a description of material condition and why in-service monitoring of the actual material is valuable.

3.5 The Stochastic Nature Of Pit Initiation And Its Bearing On The CPT

A feature of pitting that is easy to overlook when the CPT is treated as a single sharp number is that pit initiation is fundamentally a stochastic process. Even on a nominally uniform surface, pits nucleate at random times and at random locations governed by the distribution of weak sites in the passive film—inclusions, grain boundaries, film thinning and local composition fluctuations (Frankel, 1998; Szklarska-Smialowska, 1986). The result is that close to the CPT, whether a specimen shows stable pitting at any given time is a matter of chance, and the measured CPT has a statistical uncertainty that decreases as the temperature ramp slows and the surface area increases. The temperature scan rate and the specimen area must be fixed, and repeat testing is necessary; a CPT without this information is incomplete. Recent studies of duplex grades clearly show that the critical crevice temperature is a probabilistic parameter that depends on the specimen and method control and can vary by several degrees even under normal conditions (Nakhaie & Asselin, 2026a). The physics of the metastable-to-stable transition is well explained by the stochastic interpretation. The rate at which metastable pits nucleate and the probability that any one of them survives to become stable increases with temperature.

The CPT is the temperature at which the product of these two rising quantities produces at least one surviving pit in the observation window. The CPT is reproducible, despite its probabilistic nature, since the survival probability increases sharply with temperature, which reflects the strongly nonlinear dependence of the local dissolution and salt-film chemistry. The transition from 'essentially never' to 'reliably' occupies a narrow temperature range. This is crucial for our subsequent argument, as the random, bursty, increasingly correlated population of current transients that comes with a CPT approach is exactly the kind of signal that our higher-order and time-frequency methods are designed to measure, so pitting is not an obstacle to the assessment of CPT from a signal perspective but its basis.

3.6 CPT Engineering Design Criteria

Design subtracts a safety margin from the CPT, not as a maximum operating temperature. Service conditions fluctuate—chloride can concentrate in deposits, crevices can develop aggressive chemistry, oxidizing biocides increase the potential; surfaces degrade over time—and industry practice generally sets an operating temperature well below the laboratory CPT, and codes for duplex stainless steels in seawater often set limits far below the intrinsic pitting threshold to prevent crevice attack at welds and fittings. The critical crevice temperature, which is always lower than the CPT, is highly influential. The discipline is consistency: the CPT used for design should be measured in an electrolyte and by a method that is representative of or conservative with respect to the service environment. In practice, the margin used reflects the uncertainties described.

The critical crevice temperature can be ten to twenty degrees below the CPT for the same alloy, and deposits, biofilms, and weld geometries create crevices in almost any real system, so design engineers usually take the crevice temperature as the binding constraint and subtract a margin for material condition and service chemistry. A safe operating temperature in a materials standard may be far below the laboratory CPT, and this is a result of engineering judgment rather than an over-conservative limit. In-service electrochemical noise monitoring reduces these margins responsibly by reporting the actual state of the material in the real environment, replacing part of the assumed uncertainty with measurement and allowing for greater confidence at the specified temperature or a justified

relaxation of an over-conservative limit. This is the real-world benefit of this kind of analysis and methodology that we have seen in the review.

4. COMPARATIVE CRITICAL PITTING TEMPERATURE OF COMMERCIAL STAINLESS STEELS

In this section, we rank commercial stainless steels using the clarified framework of Section 3 and concentrate on super-austenitic 904L, a workhorse for moderately severe seawater duty, and hyper-duplex UNS S32707, one of the most pitting-resistant stainless steels.

4.1 Pitting Resistance Evolution And Alloy Families

Commercial stainless steels for chloride service have a pitting resistance hierarchy based on alloy content. Standard austenitic grades 304L and 316L, with PREN of roughly 18 and 24, pit readily in seawater and are unsuitable for warm chloride service; 317L and the duplex grade 2205 occupy an intermediate position; the super-austenitic grades 904L, 254 SMO and AL-6XN, together with the super-duplex grades S32750 and S32760, provide strong resistance; and the hyper-duplex grade S32707, with a PREN of about 49, sits at the top of the stainless-steel range, beyond which lie nickel-based alloys (Davis, 2000; Sedriks, 1996; Sandvik, 2007). Graph 4 shows the ferric-chloride CPT and PREN for this progression, and Graph 3 (Section 3.4) shows the underlying PREN–CPT correlation.

It is worth marking the upper boundary of the stainless-steel range explicitly, because it frames the economic logic of alloy selection. Above the hyper-duplex grades, further gains in pitting resistance require nickel-based alloys such as alloy 625 and alloy C-276, whose very high molybdenum contents give them CPT values beyond the reach of any stainless steel but at several times the material cost (Davis, 2000; Sedriks, 1996). The engineering value of a grade such as S32707 is that it approaches the pitting resistance of the least-alloyed nickel materials while retaining the far lower cost, higher strength and easier availability of a stainless steel, so that the hyper-duplex grades occupy a deliberately chosen niche between the super-austenitics and the nickel alloys (Sandvik, 2007; Chen et al., 2019). This is why an accurate, environment-specific knowledge of where each grade's CPT actually lies—rather than a conservative ferric-chloride ranking—has direct commercial value: specifying a nickel alloy where a correctly assessed hyper-duplex grade would suffice is expensive, while the reverse error is dangerous.

The measurement and monitoring methods that are the subject of this review are, in the end, tools for making that judgement on a sound basis. The same electrochemical-noise methodology extends upward to the nickel-based alloys that lie beyond the stainless range, where it has recently been applied to characterise the corrosion behaviour of a nickel-based superalloy, underlining the generality of the approach across the alloy spectrum relevant to aggressive chloride service (Jian et al., 2026).

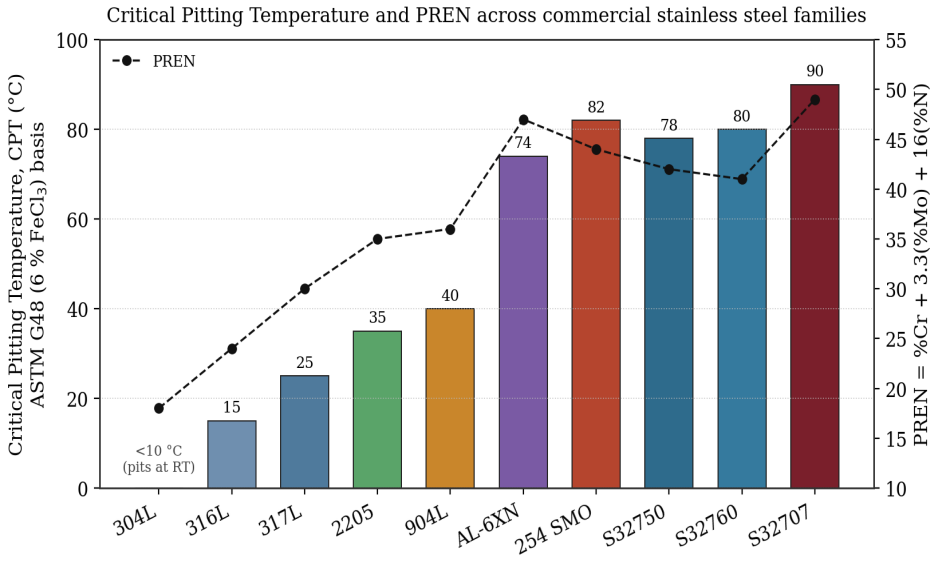

Graph 4. Critical pitting temperature and PREN across commercial stainless-steel families

Graph 4 illustrates the Ferric-chloride (ASTM G48) critical pitting temperature and pitting resistance equivalent number across commercial stainless-steel families. The two quantities rise together from standard austenitic grades through duplex and super-austenitic grades to the super-duplex and hyper-duplex grades; 904L and hyper-duplex S32707 are highlighted as the focus alloys of this review. Values are ferric-chloride results and are conservative relative to sodium-chloride service, per Section 3.3. Source: compiled by the authors from Sedriks (1996), Davis (2000), Sandvik (2007) and Xu et al. (2018).

4.2 Super-Austenitic 904L In Seawater And Brine

Alloy 904L (UNS N08904) is a high-nickel, high-molybdenum austenitic stainless steel containing approximately 20 % chromium, 24–26 % nickel, 4–5 % molybdenum and a deliberate 1–2 % copper addition (Davis, 2000). The high nickel content stabilises the austenite and confers excellent resistance to chloride stress-corrosion cracking, while the molybdenum and copper improve resistance to both chloride pitting and reducing acids, making 904L a versatile choice for seawater heat exchangers and for acid-handling duties (Davis, 2000; Sedriks, 1996). In ferric-chloride testing its CPT is modest—of the order of 40 °C by ASTM G48—consistent with its PREN of about 36, whereas in the far less aggressive sodium-chloride electrolyte its electrochemical CPT is substantially higher, which is exactly the method dependence emphasised (ATI, 2020; About Corrosion, 2013).

The behaviour of 904L in brine differs from its behaviour in seawater in ways that matter for desalination. Concentrated brine, the reject stream of reverse-osmosis and thermal desalination plants, has a higher chloride activity than feed seawater. This reduces the effective pitting threshold, but it is often deaerated and less oxidizing and therefore increases it. The final effect depends on chemistry, temperature and oxidizing biocides (Salinas-Bravo & Newman, 1994). 904L is well suited for ambient and moderately warm seawater and brine, but when it is continuously submerged, warm or chlorinated service, super-duplex and 6% molybdenum grades are better, because they have a larger safety margin against temperature excursions and deposit formation typical for operating plant. Graph 2 shows 904L and 254 SMO and S32707 for all techniques and demonstrates the true benefit of higher alloy grades and the need to not mix ferric-chloride and saltwater quantities. 904L has a better pitting resistance than duplex grades, and its CPT is less sensitive to thermal history than those of duplex grades because it is a fully austenitic alloy.

Sensitization and precipitation of intermetallic phases can occur in long periods of time in the critical temperature range. If the basis of the calculation is correct, then it is a PREN of about 36 and well above the normal 316L grade PREN of about 24, but below the super-duplex and hyper-duplex grades. In desalination applications, 904L is a well-established and easy-to-fabricate grade for cooler streams with less chloride and intermittent exposure, but higher-alloyed grades are used for hotter, more concentrated, and continuously wetted circuits where their larger CPT margin justifies their cost and fabrication.

4.3 Super-Duplex And Hyper-Duplex Grades

The duplex family combines roughly equal fractions of ferrite and austenite, achieving high strength and good stress-corrosion resistance together with pitting resistance that scales with alloy content. Super-duplex grades S32750 (25Cr–7Ni–4Mo–0.27N) and S32760 add nitrogen and, in S32760, tungsten and copper, reaching PREN of about 41–43 and ferric-chloride CPT near 75–80 °C (Davis, 2000; Nilsson, 1992). Hyper-duplex S32707 (SAF 2707 HD) pushes chromium to about 27 %, molybdenum to about 4.5 % and nitrogen to about 0.4 %, giving a PREN of roughly 49 and, under ferric-chloride conditions, a CPT reported at approximately 90 °C—higher than any standard super-duplex grade and approaching that of the 6 % molybdenum super-austenitics (Sandvik, 2007; Chen et al., 2019). This exceptional resistance, together with high strength and toughness down to low temperatures, is what qualifies S32707 for the most demanding subsea and high-chloride, high-temperature seawater applications (Sandvik, 2007).

A crucial caveat applies to all highly alloyed duplex grades: their pitting resistance is contingent on a sound microstructure. The very high chromium and molybdenum contents that give S32707 its high PREN also make it prone to rapid precipitation of sigma phase and chromium nitrides if cooling from solution treatment or welding is too slow, and such precipitation depletes the surrounding matrix of chromium and molybdenum, causing a sharp fall in the effective CPT (Chen et al., 2019; Xu et al., 2018). Since the S32707 studies always combine the CPT measurements along with the microstructural characterizations and provide the solution-annealed condition for service.

4.4 Case Study: S32707's Critical Pitting Temperature In Sodium Chloride

It is relevant to consider our review of the CPT of super-duplex/hyper-duplex S32707 in sodium chloride for the comparison of the four electrochemical methods by Xu et al. (2018). Table 3 shows that the potentiodynamic CPT is 55-65 °C, the potentiostatic CPT is 64 °C, the impedance-derived pitting temperature is 65 °C, and the electrochemical-noise CPT is 58-65 °C (Xu et al., 2018). Both conclusions follow. First, the four independent methods agree closely with one another—within a few degrees—which strongly supports the reliability of the sodium-chloride electrochemical CPT and validates the electrochemical-noise method against the established polarization and impedance techniques. Second, these sodium-chloride values are markedly lower than the roughly 90 °C obtained for the same alloy in ferric chloride, a difference that is not a contradiction but a direct illustration of the electrolyte dependence emphasised throughout Section 3: ferric chloride is far more aggressive than sodium chloride, so it drives stable pitting at a lower temperature.

For the purposes of this review the electrochemical-noise result is the most significant, because it demonstrates that a non-perturbative measurement of spontaneous fluctuations can locate the CPT as accurately as methods that impose a potential or current, while offering the additional prospect of continuous, in-service monitoring (Xu et al., 2018). The close agreement of the EN-derived CPT with the potentiostatic and impedance values in Table 3 is the empirical anchor for the analytical argument developed in Section 5, that the onset of stable pitting is written into the higher-order statistics of the noise record.

The wider significance of the S32707 case study for this review lies in what the multi-method agreement certifies. Each of the four sodium-chloride methods interrogates the pitting transition through a different observable—the collapse of the pitting potential in the potentiodynamic scan, the sustained current rise at fixed potential in the potentiostatic test, the fall in charge-transfer resistance in impedance spectroscopy, and the onset of sustained transient activity in the noise record—yet all four converge on essentially the same temperature (Xu et al., 2018). This convergence is strong evidence that they are all responding to a single underlying physical event, the stabilisation of pitting, rather than to method-specific artefacts. For the electrochemical-noise method in particular, agreement with three independent and well-established techniques provides the external validation that a passive, interpretation-dependent measurement most needs, and it justifies treating the noise-derived CPT as a legitimate determination rather than a qualitative indicator. It is on this validated footing that the higher-order analysis of the same noise signal, developed in Section 5, can be advanced with confidence: the raw material of the bispectral argument is a signal already shown to encode the CPT faithfully.

Table 3. Critical pitting temperature of hyper-duplex S32707 in sodium chloride measured by four electrochemical methods, after Xu et al. (2018), compared with the ferric-chloride value. Source: data from Xu et al. (2018).

Method	Electrolyte	Measured CPT (°C)	Basis of determination
Potentiodynamic polarization	NaCl	55–65	Temperature at which pitting potential collapses
Potentiostatic polarization	NaCl	64	Current rise above threshold at fixed potential
Electrochemical impedance (EIS)	NaCl	~65	Sharp fall in charge-transfer resistance
Electrochemical noise (EN)	NaCl	58–65	Onset of sustained pitting transients / coupling
Ferric-chloride immersion (G48)	6 % $FeCl_3$	~90	Lowest T giving visible stable pits (conservative)

NaCl values after Xu, Zhao, Feng, Li & Zhang (2018); ferric-chloride value after Sandvik (2007) / Chen et al. (2019). The close agreement of the four NaCl methods validates the EN determination against established techniques.

4.5 Seawater Versus Brine And The Role Of A Consistent Basis

Bringing the threads together, the comparison of 904L and S32707 illustrates both the genuine metallurgical progression in pitting resistance and the interpretive discipline that must accompany any CPT comparison. On a continuous ferric-chloride basis S32707 (~90 °C) dominates 904L (~40 °C). For a constant sodium-chloride electrochemical basis S32707 (58–65 °C) leads 904L, however, the absolute values and gap depend on the environment. Desalination brine is higher in chloride but less oxidizing than aerated seawater, so the CPT should be assessed in that environment or conservatively. Electrochemical noise is more attractive for this application because it can be used in the service

electrolyte and temperature and is therefore less like a laboratory ranking but more in the field (Xu et al., 2018). The threshold is also affected by brine chemistry, as in mixed chloride-sulfate media typical of many process and hydrometallurgical streams the more chloride-chloride the critical pitting and critical crevice temperatures of 2205 duplex stainless steel are increased, so a chloride-only assessment is more conservative for real brines.

4.6 Seawater And Desalination Material Selection

The comparison of 904L to S32707 is important when engineers decide on stainless steels for seawater intake systems, heat-exchanger tubing, reverse-osmosis high-pressure circuits, and desalination plant brine-reject lines. Because the CPT creates a ceiling that reduces the safety margin as the process warms and chloride concentrates under scale and biofilm, temperature generally determines these duties. A material whose seawater CPT sits only a little above the maximum process temperature offers no protection against the transient excursions, crevices and deposit-covered surfaces that real plant inevitably presents, whereas one whose CPT lies well above the process temperature tolerates these upsets. This is why the several tens of degrees that separate 904L from S32707 translate into markedly different service envelopes, and why the hyper-duplex grade is reserved for the hottest, most concentrated and most safety-critical circuits despite its higher cost and more demanding fabrication (Sandvik, 2007; Chen et al., 2019).

Two practical lessons follow from the method-dependence argument of Section 3.3 when it is applied to selection. The first is that alloys must be ranked on a consistent basis: comparing a ferric-chloride CPT for one grade with a sodium-chloride electrochemical CPT for another can invert the true ordering and lead to an unsafe choice. The second is that the laboratory value used for selection should be, if not measured in the actual service electrolyte, at least conservative with respect to it; and because brine and chlorinated seawater differ from the standard test solutions, a residual uncertainty always remains. It is precisely this residual uncertainty that motivates in-service, non-perturbative monitoring of the kind that electrochemical noise makes possible, so that the margin assumed at the design stage can be verified—or corrected—against the behaviour of the actual material in the actual environment (Xu et al., 2018; Hou et al., 2017). The comparative CPT data of this section thus lead naturally to the monitoring methodology developed in Sections 5 to 7.

5. THE RELATIONSHIP BETWEEN ELECTROCHEMICAL NOISE AND BISPECTRUM ANALYSIS FOR STAINLESS STEEL

This section develops the central analytical argument of the review: that the transition from metastable to stable pitting which defines the CPT is a nonlinear process whose signature is expressed far more clearly in the bispectrum of an electrochemical-noise record than in its mean current, noise resistance or power spectrum. The argument proceeds from the physics of pit interaction, through the evolution of the raw noise record, to the emergence of quadratic phase coupling in the bispectrum, and closes with the quantitative descriptors that connect bispectral features to the CPT and with the supporting experimental evidence.

5.1 Why Pitting Is A Nonlinear, Non-Gaussian Process

Recall from Section 2.4 that the bispectrum is identically zero for a Gaussian, linear process and becomes non-zero only when a signal contains non-Gaussian, phase-coupled structure. The question, therefore, is whether the electrochemical noise of a pitting stainless steel possesses such structure, and if so, when. The mechanistic picture of Section 3.2 supplies the answer. Well below the CPT, passive-film rupture events are small, rare and self-healing; each nucleates and repassivates independently of the others, because a pit that repassivates within milliseconds does not appreciably alter the environment experienced by its neighbours. A population of such independent, randomly timed micro-events approximates a Gaussian, linear stochastic process, and its bispectrum is therefore close to zero (Darowicki & Zieliński, 2008).

As temperature rises toward the CPT this independence breaks down. Metastable pits survive longer, grow larger and, crucially, begin to modify their surroundings: each growing pit acidifies the adjacent electrolyte, accumulates chloride and depletes oxygen over a diffusion field that overlaps those of its neighbours (Galvele, 1976; Laycock & Newman, 1997). A pit that has locally lowered the pH makes it easier for a nearby site to nucleate and harder for it to repassivate, so events become positively correlated in space and time. The frequency components of the noise record have fixed phase correlations due to this mutual reinforcement, which is a nonlinear interaction. So the signal is non-Gaussian and phase-coupled, which is detected by the bispectrum (Darowicki & Zieliński, 2008; Nikias & Petropulu, 1993).

Be explicit about the two statistical departures the bispectrum finds because they enter the pitting problem at different phases. A record with rare, massive, one-sided transients is non-Gaussian even if they are independent and still has a non-zero bispectrum. Nonlinear phase coupling is stronger and more specific: only when events interact do frequency components have definite phase connections. The first departure occurs when discrete metastable transients dominate the record before the CPT and the second is the actual signature of cooperative behavior where the pits interact around the CPT. A rigorous bispectral analysis can separate these two contributions, and the normalized bicoherence is the better coupling component measure as it does not impact the overall amplitude that dominates the non-Gaussianity contribution (Collis et al., 1998). This is indeed consistent with the main point of the review that phase coupling, not huge transients, is what separates the CPT approach more clearly.

5.2 CPT Raw Noise Record Evolution

Prior to changing the signal, the raw record should be analyzed as these will have to be made visible to the higher level of the signal. Figure 5: Current-noise record evolution in three regimes. Below the CPT, the record is quiet: small, symmetric fluctuations in a stable mean, sometimes marked by a brief transient that decays quickly as the film is repaired. In the presence of a strong metastable pitting at the CPT, the record is intermittent with frequent, bigger transients whose decay gets longer as repassivation becomes less certain. Large irregular excursions that no longer recover dominate the record above the CPT. This suggests that the record is permanently broken at stably propagating holes (Pistorius & Burstein, 1992; Aballe et al., 2001). When discrete events dominate the record, kurtosis and localization increase, and noise is not very strong in Section 2.2. These first order and second-order measures, however, register that something has changed without distinguishing a population of independent large events from a population of coupled ones. A record of many independent transients and a record of the same number of mutually reinforcing transients can share similar variance, kurtosis and power spectrum, yet they represent physically different states—one a benign shower of metastable pits, the other the onset of cooperative, stable pitting. Discriminating between them requires a phase-sensitive measure, and this is the specific contribution of the bispectrum.

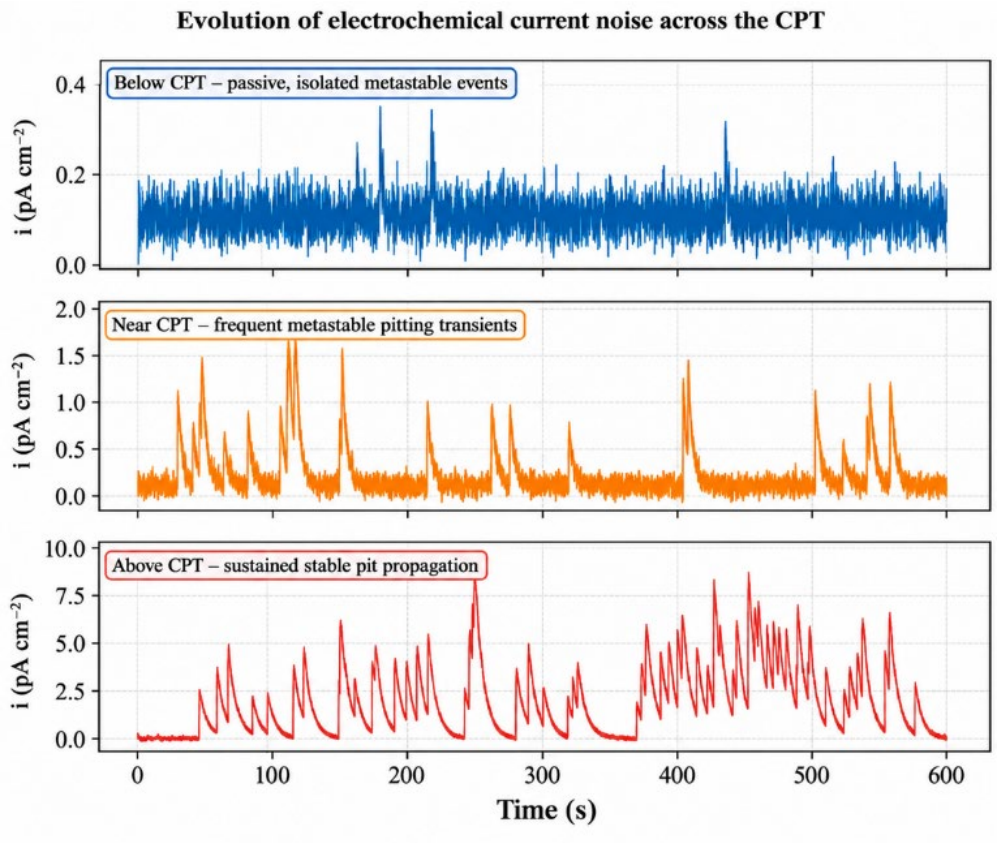

Graph 5. Evolution of electrochemical current noise across the CPT

Graph 5 are representative evolution of the electrochemical current-noise record for a stainless steel as temperature crosses the critical pitting temperature. Below the CPT (top) the record is quiet with rare, rapidly repairing transients; near the CPT (middle) frequent, longer-lived metastable transients appear; above the CPT (bottom) large, incompletely recovering excursions reflect stable pit propagation. The change in event statistics motivates higher-order analysis. Source: schematic prepared by the authors after Pistorius and Burstein (1992).

5.3 Emergence Of Quadratic Phase Coupling In The Bispectrum

Applying the power spectrum to these records shows the expected changes—an increase in low-frequency power and a steepening of the roll-off slope as slow, large transients come to dominate in Graph 6 but, as argued in Section 2.3, the power spectrum discards the phase and so cannot reveal whether the events are coupled. The bispectrum, which retains the phase, tells a much richer story. Figure 7 shows the characteristic evolution of the bispectrum magnitude surface across the three regimes. Below the CPT the surface is flat and featureless apart from low-amplitude scatter, the signature of a near-Gaussian process in which the frequency components are essentially independent. Near the CPT discrete peaks rise out of the bifrequency plane, marking the appearance of quadratic phase coupling as pits begin to interact. Above the CPT these peaks become intense and organised, concentrated at the frequencies characteristic of the cooperative dissolution processes that sustain stable pits (Darowicki & Zieliński, 2008).

It is natural to ask what sets the particular frequencies at which the bispectral peaks appear, since their location, not only their height, carries information. The characteristic frequencies of an electrochemical-noise record reflect the time constants of the underlying events: the rapid rise and slower decay of an individual metastable transient define a band in the tens-of-hertz to sub-hertz range, while the slower modulation associated with the growth and partial repair of stable pits appears at lower frequencies (Pistorius & Burstein, 1992; Darowicki & Zieliński, 2008). Quadratic phase coupling between a low-frequency modulation and a higher-frequency transient band therefore produces bispectral peaks at bifrequencies determined by these physical time constants, and the migration of the peaks toward lower bifrequencies as stable pitting develops parallels the migration of wavelet energy toward coarser crystals described in Section 6. The two representations are thus complementary views of the same physical slowing and organisation of the dominant events: the wavelet transform expresses it as a shift in the timescale carrying the most energy, and the bispectrum expresses it as a shift in the frequencies that are phase-coupled. Recognising this correspondence is what allows the descriptors from the two transforms to be interpreted jointly rather than as unrelated numbers.

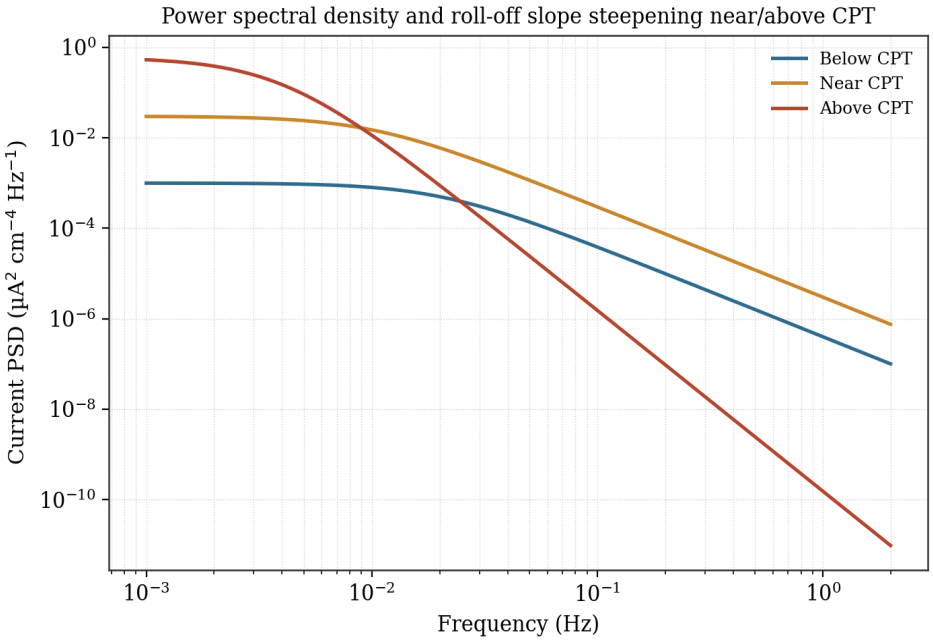

Graph 6. Schematic evolution of the current power spectral density across the CPT

Graph 6 displays the schematic evolution of the current power spectral density across the CPT the low-frequency power rises and the high-frequency roll-off steepens as slow, large transients come to dominate. The power spectrum registers the change in event character but, retaining only magnitude and not phase, cannot reveal whether the underlying events are coupled. Source: schematic prepared by the authors.

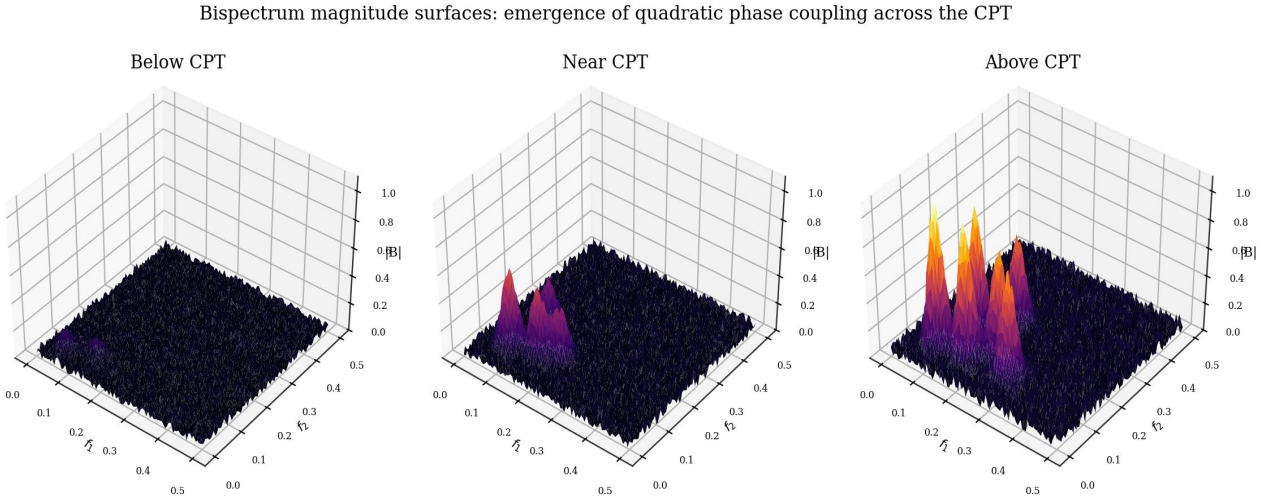

Graph 7. Bispectrum magnitude surfaces

Graph 7 shows the bispectrum magnitude surfaces of the electrochemical-noise record below, near and above the critical pitting temperature. The near-Gaussian, uncoupled behaviour below the CPT produces a flat surface; discrete peaks emerge near the CPT as quadratic phase coupling appears between frequency components; and intense, organised peaks dominate above the CPT, reflecting the cooperative dissolution of stably propagating pits. Source: schematic prepared by the authors after Darowicki and Zieliński (2008).

The physical interpretation of these peaks is important. A peak at a bifrequency (f_1, f_2) indicates that oscillatory activity at f_1 and f_2 is phase-locked to activity at their sum, as occurs when a nonlinear process transfers energy between scales with a preserved phase relationship (Nikias & Petropulu, 1993). In the pitting context this corresponds to the synchronisation of dissolution transients as neighbouring pits couple via their common local chemistry: the coupling gives rise to fluctuation energy at combination frequencies that a linear sum of independent events could not produce. These peaks therefore offer a direct physical readout of the transition from independent metastable events to cooperative stable pitting (i.e., crossing the CPT).

5.4 Quantitative Bispectral Descriptors And Their Relationship With CPT

The two-dimensional bispectrum surface can be reduced to a scalar descriptor and can be measured against temperature. The intensity of the bispectral peak determines the height of the dominant coupling peak and rises high as stable pitting starts; the bispectral energy is a function of the bifrequency of the coupling and falls as activity is concentrated into a few strong peaks (Nikias & Petropulu, 1993; Collis et al., 1998). The bicoherence, being normalised, is particularly useful for comparing coupling strength between alloys or conditions with different overall noise levels.

Plotted against temperature, these descriptors remain low and flat while the surface is featureless and then rise sharply as the coupling peaks emerge, so the temperature at which a descriptor crosses a chosen threshold provides a bispectral estimate of the CPT. Because more pitting-resistant alloys maintain an uncoupled, near-Gaussian noise character to higher temperatures—their stable passive films suppress the interaction of metastable events—the temperature at which their bispectral descriptors rise is correspondingly higher, so that the bispectral-onset temperature ranks alloys in the same order as their CPT. In this way the qualitative surfaces of graph 7 become a quantitative CPT criterion, and the descriptors become features suitable for the data-driven models of Section 2.6 and the integrated workflow of Section 7.

The shape of the descriptor-versus-temperature curve carries information beyond the crossing point itself. A gradual, early rise in bispectral energy that precedes the sharp rise associated with stable pitting reflects the growing but still incomplete organisation of the metastable population, and the temperature separation between this early rise and the conventional current-based CPT is a direct measure of the early-warning margin that higher-order analysis offers. Where a temperature ramp is followed by cooling, comparison of the heating and cooling descriptor curves can reveal hysteresis: once stable pits have formed, the coupled activity may persist to temperatures below the CPT because established pits maintain their own aggressive chemistry, mirroring the well-known gap between the pitting and repassivation potentials (Frankel, 1998; Laycock & Newman, 1997). Such hysteresis is potentially diagnostic in its own right, as it distinguishes a surface that is only at a stage of instability from one on which stable pits are already well developed. These properties imply that the bispectral descriptors are valuable not only to provide a new CPT number but also to give insight into the state and history of a corroding surface more accurately than one temperature as a threshold.

5.5 Experimental Evidence Linking EN And The Bispectrum In Stainless Steels

The correlation between electrochemical noise and higher-order analysis of stainless-steel pitting is not only theoretical but also experimental. Darowicki and Zieliński (2008) studied an austenitic stainless steel in ferric-chloride solution and showed in an integrated form that the bispectrum (and hence more than that) could provide information about the presence and time constant of current transients associated with metastable pitting that would not be available for spectra of the present state, and they explicitly proposed the third-order cumulant and bispectrum to be used as detectors for nonlinear parts of the noise (Darowicki & Zieliński, 2008). This is precisely the mechanism argued for above: the bispectrum captures the phase-coupled, non-Gaussian structure that accompanies pit interaction.

The validation of the electrochemical-noise CPT of S32707 by Xu et al. (2018) closes the loop from the opposite direction. Their finding that the EN-derived CPT (58–65 °C) agrees with the potentiostatic and impedance values demonstrates that the onset of stable pitting is faithfully recorded in the noise signal; combined with the bispectral mechanism, this implies that the same onset should be locatable—and, on the argument above, locatable earlier—through higher-order analysis of that signal (Xu et al., 2018; Darowicki & Zieliński, 2008). More broadly, the wider literature that applies statistical, spectral and wavelet analysis to the EN of austenitic and duplex stainless steels consistently reports a systematic change in the character of the noise as localized corrosion sets in, providing the empirical backdrop against which the specific sensitivity of the bispectrum to inter-event coupling stands out (Aballe et al., 2001; Suresh & Kamachi Mudali, 2014). The practical promise is early warning: because coupling appears as the population of metastable pits begins to organise—before any single pit dominates the mean current—a bispectral criterion can signal the approach to the CPT sooner than criteria based on average current or polarization resistance (Darowicki & Zieliński, 2008).

5.6 Methodological Considerations For Reliable Bispectral Estimation

The diagnostic value of the bispectrum for CPT assessment is real, but it is contingent on sound estimation practice, and several methodological points deserve emphasis if the descriptors of Section 5.4 are to be comparable between studies. The first concerns data length. Because the bispectrum is a two-dimensional function estimated from third-order statistics, it is far more data-hungry than the power spectrum; reliable estimates require long, quasi-stationary records divided into many overlapping segments whose bispectra are averaged, and short records yield noisy surfaces in which spurious peaks can be mistaken for genuine coupling (Nikias & Petropulu, 1993; Collis et al., 1998). The requirement of quasi-stationarity is in tension with the non-stationary nature of a temperature ramp, so a compromise must be struck between segments long enough for stable estimation and short enough that the surface state does not change appreciably within them—a compromise the wavelet transform, being explicitly time-resolved, helps to manage.

The second is pre-processing. Detrending and drift removal, which is critical for any spectral estimate, can affect the low frequency phase structure for the bispectrum and so the choice of detrending method can affect the coupling. Wavelet removal of the smooth part has been used by some for higher order of work, because it can remove the drift without a polynomial phase distortion (Aballe et al., 1999; Homborg et al., 2012). The last point is normalization. The magnitude of the bispectral depends on the overall energy of the record and coupling of alloys or temperatures should be compared using the bicoherence, which is the separation of that energy to be the phase-

coupling part (Collis et al., 1998). Finally, the bispectral CPT criteria should be clearly defined and it should be balanced with a conventional potentiostatic or impedance measurement in the same electrolyte (e.g., the multi-method verification of Xu et al., 2018) and the study of these points is what distinguishes a reproducible bispectral CPT from an artefact of estimation, and their standardization is one of the research gaps that we address in section 7.

It is interesting to point out that the diagnostic logic we use here is not unique to corrosion but borrowed from fields where higher order analysis is quite well established. In mechanical fault detection, the appearance of bispectral peaks signals the nonlinear coupling which accompanies incipient gear or bearing damage; in fluid dynamics, bicoherence indicates the onset of the wave interaction that precedes turbulence; and in biomedical signal processing, higher order spectra signal the transition of physiological states (Nikias & Petropulu, 1993; Collis et al., 1998). In each case the method is successful for the very same reason that it will work for pitting: a system approaching a change of regime starts to couple its degrees of freedom and that coupling is written into the phase structure of the signal before it dominates the signal. The transfer of this mature methodology to the electrochemical noise of stainless steels is therefore not a speculative analogy but the application of a general principle to a system which already meets its preconditions - nonlinearity, non-Gaussianity and a threshold transition. Recognising the pitting problem as one instance of a broad class of regime-change detection problems both explains why the bispectral approach should work and connects corrosion science to a large body of signal-processing experience on which it can draw.

6. WAVELET AND INTEGRATED TIME–FREQUENCY SIGNATURES OF PITTING

The bispectrum reveals that pitting events become coupled as the CPT is approached, but it does not, by itself, say when in the record those events occur or on what timescale they act, because it is a stationary, frequency-domain measure. The wavelet transform supplies exactly this missing information and is therefore the natural complement to higher-order analysis (Aballe et al., 1999; Homborg et al., 2012).

6.1 Migration Of Wavelet Energy From Fine To Coarse Crystals

As described in Section 2.5, the discrete wavelet transform decomposes an EN record into detail crystals D1–D8 and a smooth residual S8, and the energy distribution plot summarises which timescales dominate. In the passive regime the energy is spread toward the finer crystals, reflecting rapid film-repair events; as metastable and then stable pitting develop, the energy migrates toward the coarser crystals D5–D8, reflecting the longer-lived, larger transients of growing pits (Suresh & Kamachi Mudali, 2014; Cardenas-Barrera et al., 2024). Suresh and Kamachi Mudali (2014), studying Type 304L in ferric chloride, reported that the medium-timescale crystal D5 dominated during the initial stages of immersion but that, as exposure continued, the maximum energy concentrated on the coarse D8 crystal, which they identified with the dominance of stable pitting. Figure 8 illustrates this migration schematically for the three regimes.

The physical mapping that gives this migration meaning—fine crystals (D1–D3) to rapid metastable events, intermediate crystals (D4–D6) to localized processes of intermediate duration, and coarse crystals (D7–D8) to slow, diffusion-controlled processes—has been applied across a range of alloys and electrolytes, and provides a timescale-resolved account of the same transition that the bispectrum describes in terms of coupling (Cardenas-Barrera et al., 2024; Suresh & Kamachi Mudali, 2014). The complementary standard-deviation-of-partial-signals plot adds sensitivity to the frequency of the predominant transients and hence to pit density (Shahidi et al., 2011).

Reducing this qualitative migration to a quantitative criterion is straightforward in principle. The fraction of total wavelet energy residing in the coarse crystals—for instance the summed energy of D6 through D8 expressed as a proportion of the whole—rises monotonically as stable pitting develops and can be tracked against temperature in exactly the way described for the bispectral descriptors, so that the temperature at which the coarse-crystal energy fraction crosses a chosen level provides a wavelet-based estimate of the CPT (Suresh & Kamachi Mudali, 2014; Cardenas-Barrera et al., 2024). The particular attraction of the wavelet energy fraction as a criterion is its robustness: unlike the bispectrum it does not require long stationary records, so it can be evaluated on shorter windows and can follow a rapid temperature ramp more faithfully, which makes it a useful real-time complement to the more data-hungry higher-order descriptors in the integrated workflow of Section 7 (Shahidi et al., 2011; Homborg et al., 2012).

Natural Resources for Human Health
eISSN: 2583-1194

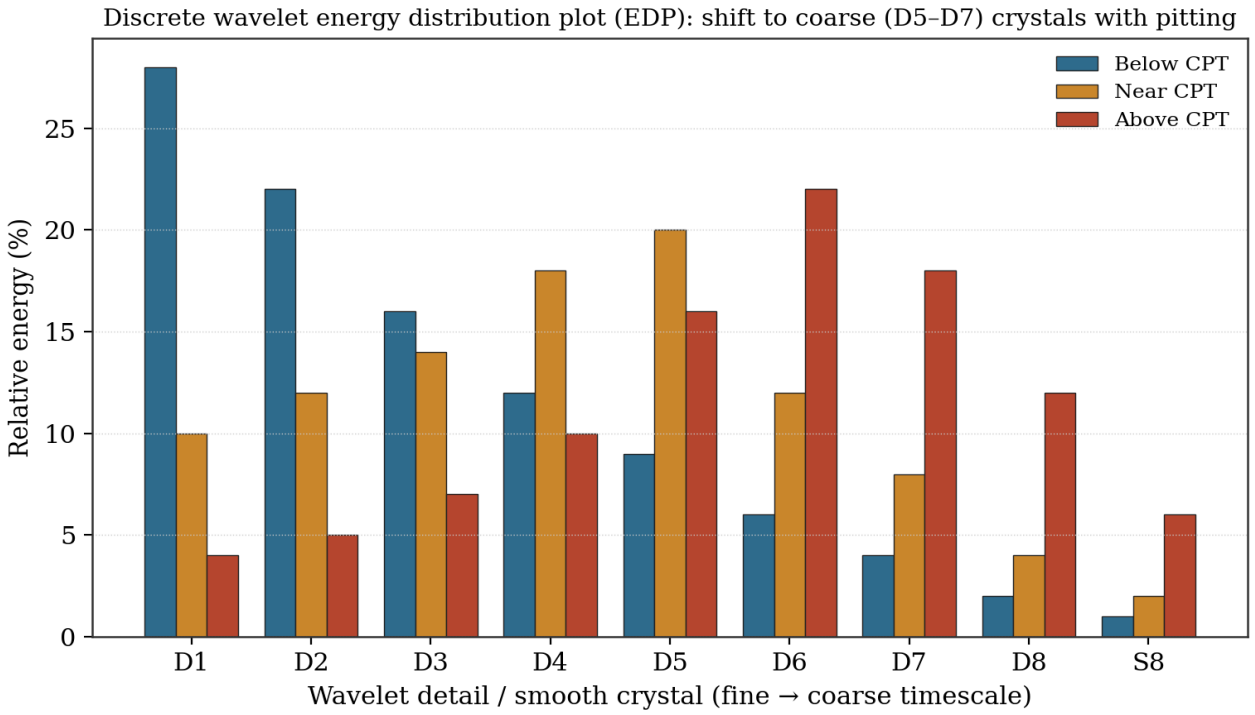

Graph 8. Schematic discrete-wavelet energy distribution plot (Suresh & Kamachi Mudali, 2014; Cardenas-Barrera et al., 2024)

Graph 8 shows the schematic discrete-wavelet energy distribution plot for a stainless steel below, near and above the critical pitting temperature. Below the CPT the energy is concentrated in the fine crystals (rapid film-repair events); near and above the CPT the maximum energy migrates to the coarse crystals (D5–D8), signalling the dominance of longer-lived, larger transients associated with stable pit propagation, consistent with the observations of Suresh and Kamachi Mudali (2014). Source: schematic prepared by the authors after Suresh and Kamachi Mudali (2014).

6.2 Wavelet Effects Of Alloying And Its Complementarity With The Bispectrum

Wavelet analysis is also sensitive to the metallurgical factors that set the CPT. Studies of the effect of nitrogen on the pitting of stainless steel using wavelet analysis have found that increasing the nitrogen content shifts energy away from the long-timescale crystals and reduces the inferred pit density, consistent with nitrogen's known role in stabilising the passive film and buffering pit chemistry (Upadhyay et al., 2022). This means that the wavelet energy distribution not only tracks the onset of pitting with temperature but also reflects the compositional resistance of the alloy, connecting the signal-analysis picture back to the metallurgy of Section 3.4.

The essential point for this review is that the wavelet and higher-order descriptions are complementary rather than redundant. The bispectrum answers whether the events are coupled—the diagnostic of cooperative, stable pitting—while the wavelet transform answers when and on what timescale they occur—the diagnostic of the character and duration of the events. A record can show migration of wavelet energy toward coarse crystals without strong bispectral coupling, indicating large but still largely independent events, or it can show both, indicating organised stable pitting. Combining the two therefore resolves states that either alone would confuse, which is the rationale for the fused feature vector of the integrated methodology developed next (Cardenas-Barrera et al., 2024; Suresh & Kamachi Mudali, 2014).

The complementarity can be made concrete by considering how the two transforms respond to a well-defined change in the corrosion state. Suppose an alloy is held just below its CPT and the temperature is nudged upward by a few degrees. If the response is simply that existing metastable events grow larger without becoming more correlated, the wavelet energy shifts toward coarser crystals but the bicoherence remains low—the events are bigger but still independent, and no stable pitting need follow. If instead the events begin to couple, the bicoherence rises sharply even before the wavelet energy shift is pronounced, flagging the onset of the cooperative behaviour that precedes stable pitting (Darowicki & Zieliński, 2008; Suresh & Kamachi

Mudali, 2014). Reading the two descriptors together clearly distinguishes a benign increase in event magnitude from the genuine approach to instability, which ultimately has a direct practical value that neither descriptor can draw alone. This is precisely what the wavelet transform provides and the bispectrum is complementary rather than redundant and why the integrated approach of Section 7 treats their descriptors as jointly necessary inputs rather than interchangeable ones.

6.3 Entropy, Recurrence And Combined Time-Frequency Descriptors

In addition to the energy distribution, a few other measures can be used to extend the scope of time-frequency analysis and strengthen its complementarity with the bispectrum. The wavelet entropy is calculated as a function of the energy distribution among the crystals. The wavelet entropy of a passive surface with a wide energy distribution over different scales are high wavelet entropy, whereas the stable pitting of the crystals concentrates the energy on a few coarse crystals and reduces the wavelet entropy. The fall in wavelet entropy therefore parallels the fall in bispectral entropy noted in Section 5.4, the two measures capturing the same organisation of the process from the timescale and phase-coupling viewpoints respectively (Shahidi et al., 2011; Cardenas-Barrera et al., 2024). Because both entropies respond to the transition, their joint use provides a more robust criterion than either alone.

Recurrence quantification analysis offers a further, geometry-based view of the same signals. By embedding the noise record in a phase space and examining the pattern of recurrent states, it produces measures—determinism, laminarity and the length of diagonal structures—that are sensitive to the shift from irregular, stochastic passive fluctuations to the more deterministic, structured behaviour that accompanies stable localized corrosion (Hou et al., 2017). Applied to electrochemical noise, recurrence analysis has been shown to track the development of localized corrosion and to feed naturally into machine-learning classifiers, and it is attractive precisely because it makes no assumption of stationarity or linearity (Hou et al., 2017; Calabrese et al., 2023). Taken together, the wavelet energy distribution, wavelet entropy, recurrence measures, bispectral descriptors and conventional statistics form a rich, partly redundant feature set. The redundancy is beneficial: it allows cross-validation between descriptors derived from different mathematical principles, so that a CPT inferred simultaneously from coarse-crystal wavelet energy, from bispectral peak onset and from a rise in recurrence determinism carries far more confidence than one drawn from a single measure. This multi-descriptor redundancy is the technical foundation of the integrated methodology developed in the next section (Cardenas-Barrera et al., 2024; Calabrese et al., 2023).

7. TOWARD AN INTEGRATED METHODOLOGY FOR CPT DIAGNOSIS AND PREDICTIVE MONITORING

The preceding sections argued that electrochemical noise carries a faithful record of the metastable-to-stable pitting transition; that the bispectrum is the natural tool for detecting the nonlinear coupling that marks the onset of stable pitting; and that the wavelet transform resolves the timescale and character of the events. This section draws these threads into a single, practical workflow for estimating the CPT and for providing early warning of localized corrosion, and it identifies what an ideal implementation would require.

7.1 An Acquisition-To-Prediction Workflow

Figure 9 sets out the proposed workflow. It begins with the simultaneous acquisition of potential and current noise from a stainless-steel specimen or component in the service electrolyte—seawater or brine—while the temperature is ramped through the region of interest. The raw records are conditioned by removing direct-current drift, detrending and segmenting into quasi-stationary windows, from which the noise resistance and basic statistics are computed. Each window is then analysed in parallel by the three complementary transforms: higher-order analysis yields the bispectral peak intensity, energy and entropy and the bicoherence; wavelet analysis yields the crystal energies and the energy distribution plot; and power-spectral analysis yields the roll-off slope and corner frequency. Together with the time-domain statistics, these form a fused feature vector describing the state of the surface in each window (Cardenas-Barrera et al., 2024; Hou et al., 2017).

The feature vector is then mapped to an interpretation. In the simplest implementation the temperature at which a chosen descriptor—bispectral peak intensity, or the coarse-crystal wavelet energy—crosses a threshold provides a direct CPT estimate, cross-checked against the conventional current or impedance criterion. In a data-driven implementation the fused features are supplied to a regression or classification model trained on labelled data to output a CPT estimate, a probability of stable pitting and, ultimately, a corrosion-state variable suitable for a digital twin (Hou et al., 2017; Chen et al., 2019). Because the higher-

order features respond to coupling as the metastable population begins to organise, such a model can in principle signal the approach to the CPT before the mean current departs from its passive value, converting a laboratory measurement into an early-warning capability.

A word on physical deployment connects the workflow to real plant. In the laboratory the noise is acquired from a small coupon, but in service the same principle can be realised with a dedicated electrochemical-noise probe—typically a set of nominally identical electrodes of the plant alloy exposed to the process stream—whose potential and current fluctuations are logged continuously. Such probes are already used for general corrosion monitoring, and the analytical layer proposed here would add higher-order and wavelet processing to the data they generate rather than requiring new hardware (Cottis, 2001; Hou et al., 2017). The temperature ramp that defines a CPT determination in the laboratory is, in service, replaced by the natural variation of process temperature: as the plant warms and cools through its duty cycle, the probe samples the alloy's response across a range of temperatures, and the descriptors can be tracked against the logged temperature to reveal whether the surface is approaching its coupling threshold. In this way a determination that is deliberate and ramp-driven in the laboratory becomes opportunistic and condition-driven in the field, but the underlying signal signature—the emergence of phase coupling and the migration of wavelet energy—is the same, which is what makes the laboratory calibration transferable to service (Xu et al., 2018; Cardenas-Barrera et al., 2024).

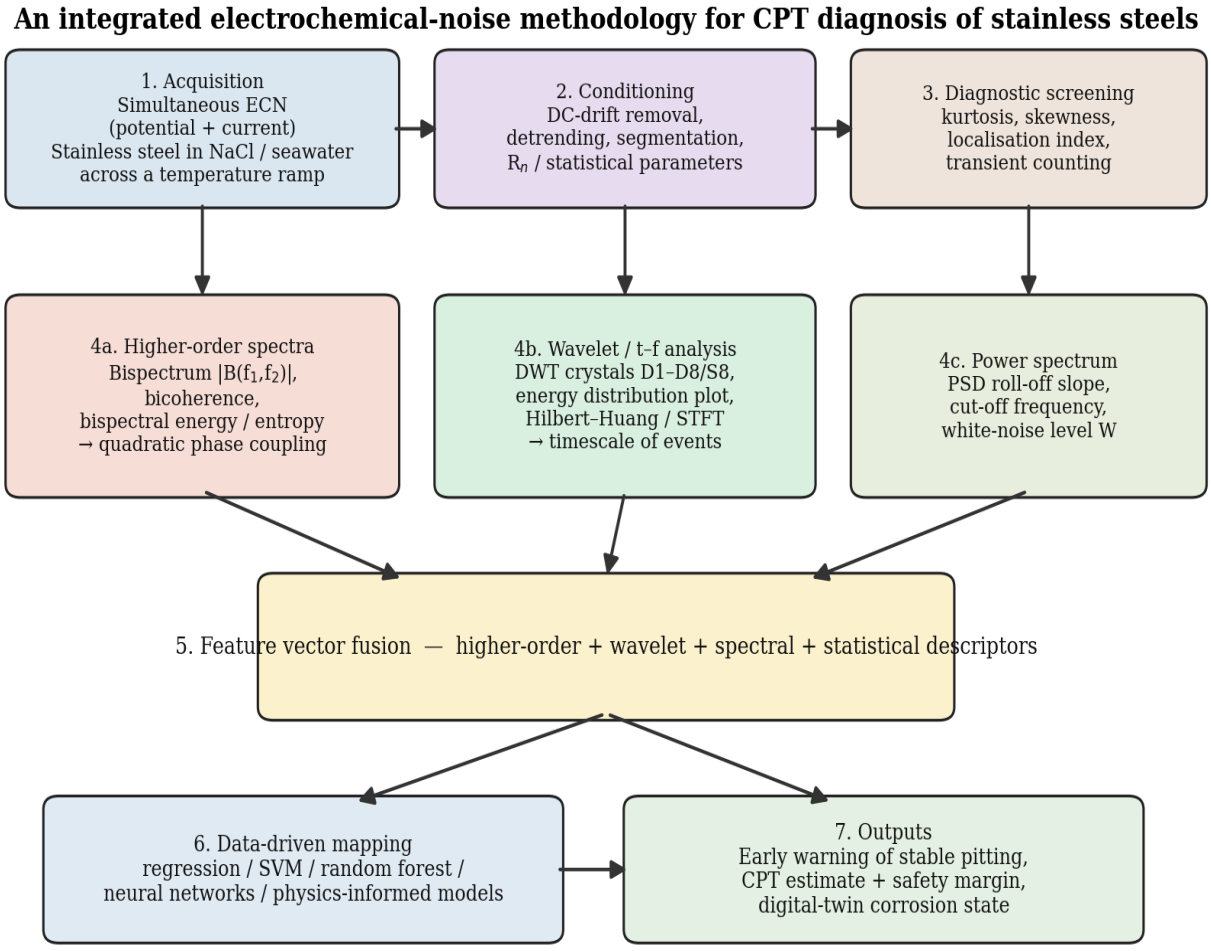

Figure 1. the proposed integrated electrochemical-noise methodology for CPT diagnosis of stainless steels

Figure 1 illustrates the proposed integrated electrochemical-noise methodology for diagnosing the critical pitting temperature of stainless steels. Simultaneous potential and current noise are acquired in the service electrolyte across a temperature ramp, conditioned, and analysed in parallel by higher-order (bispectral), wavelet and spectral transforms; the fused feature vector is mapped by physically motivated thresholds or data-driven models to a CPT estimate, an early warning of stable pitting and a corrosion-state variable for condition-based maintenance and digital twins. Source: original figure prepared by the authors.

7.2 Requirements, Limitations And The Ideal Implementation

An ideal implementation of this workflow would satisfy several conditions that current practice only partly meets. First, it demands high-quality, low-noise acquisition with a sampling rate and record length sufficient to resolve the transients of interest and to support reliable estimation of a two-dimensional bispectrum, which is intrinsically data-hungry (Nikias & Petropulu, 1993; Bertocci et al., 1997). Second, it requires principled signal conditioning, since the low-frequency content that carries much of the pitting information is also where drift contaminates the record, and wavelet-based detrending is attractive because it can separate drift from signal within the same framework used for analysis (Aballe et al., 1999). Third, the mapping from features to CPT should consider the standard determinations as Xu et al. (2018) did for S32707 for each alloy and electrolyte to evaluate the data due to the quantification of bispectral onset and the standard CPT being not universal (Xu et al., 2018; Cardenas-Barrera et al., 2024). There are several limitations: the higher-order estimation is sensitive to record length and windowing, the wavelet-mechanism mapping is experimental and depends on the analysing wavelet, and data-driven models cannot consistently transfer data between conditions (see section 2.6). Faint and noisy electronics and biofilm formation are also important for field monitoring and so monitoring will require the integration of multiple descriptors in the environment so that no one perturbation can be used to explain in-service (Calabrese et al., 2023; Cardenas-Barrera et al., 2024). All these caveats aside, the combination of a validated electrochemical-noise CPT, a physically anchored higher-order detector of the pitting transition, and a mature machine-learning toolkit makes the integrated methodology a realistic near-term goal rather than a speculative one, and puts electrochemical noise as the sensing approach of choice to digital corrosion management of stainless steels in seawater and brine (Xu et al., 2018; Chen et al., 2019).

7.3 A Proposed Validation Programme And Research Priorities

To take the integrated methodology from a proposal to an accepted engineering tool requires a programme of work and it is useful to state its elements. The first priority is a systematic bispectral and wavelet study of the highly alloyed grades that matter for seawater and desalination service—904L, the super-duplex grades and hyper-duplex S32707—across controlled temperature ramps in both sodium chloride and realistic brine, with the higher-order and time–frequency descriptors recorded in parallel with a conventional potentiostatic determination. Such a study would establish, for the alloys of practical interest, the quantitative relationship between the bispectral-onset temperature and the standard CPT criterion, which at present has been demonstrated in detail only for a limited set of materials (Xu et al., 2018; Darowicki & Zieliński, 2008).

The second priority is standardisation. For signal-based CPT criteria to be comparable between laboratories, the community needs agreed conventions for acquisition parameters, drift removal, windowing and higher-order estimation, together with a defined descriptor and threshold for the bispectral CPT, in the same way that ASTM G150 fixed the potential, scan rate and current criterion for the potentiostatic method (ASTM International, 2020). Without such conventions the sensitivity of higher-order descriptors to pre-processing, discussed in Sections 2.8 and 5.6, will continue to produce apparently conflicting results. The third priority is field validation: controlled laboratory ramps must be complemented by long-duration monitoring on operating plant, under the fouling, flow and biofilm conditions that laboratory tests omit, so that the robustness of a fused-feature criterion can be assessed against real service data (Hou et al., 2017; Calabrese et al., 2023). The fourth priority is the development and open sharing of labelled datasets and trained models, since the data-driven layer of the workflow can only mature if models can be trained, tested and transferred across alloys and environments (Cardenas-Barrera et al., 2024; Calabrese et al., 2023). Progress on these four fronts would convert the physically motivated but still largely qualitative picture assembled in this review into a quantitative, standardised and field-proven capability.

Underlying all four priorities is a need for closer collaboration between the corrosion-science and signal-processing communities, which have historically published in separate venues and adopted different conventions. The bispectral and wavelet methods at the heart of this review were developed and refined largely outside corrosion, while the

mechanistic knowledge of the CPT was developed largely outside signal processing, so it is essential that practitioners work in both fields. Common datasets, reporting standards and benchmarking exercises would facilitate this convergence, and the relatively well-defined CPT problem with a clear physical threshold and its economic significance in desalination and marine engineering would make for a perfect platform for the two fields to work together in a common language.

8. CONCLUSIONS AND OUTLOOK

This review has connected two literatures that are usually kept apart—the signal analysis of electrochemical noise and the pitting metallurgy of stainless steels—around the specific problem of the critical pitting temperature. The principal conclusions are as follows.

First, treated as signal-processing tools in their own right, electrochemical noise, the power spectrum, the bispectrum and the wavelet transform play complementary and non-interchangeable roles: the power spectrum describes energy versus frequency but discards phase; the bispectrum recovers phase coupling and hence nonlinearity and non-Gaussianity; and the wavelet transform localises energy in time and scale. Their combination, rather than any one alone, gives the most complete description of a corroding surface.

Second, the critical pitting temperature is a genuinely reproducible threshold that marks the metastable-to-stable pitting transition, but reported values are meaningful only when the test method and electrolyte are stated. Ferric-chloride (ASTM G48) values are conservative and best used for ranking and defect detection, whereas potentiostatic (ASTM G150) and other electrochemical values in sodium chloride are higher and more design-relevant; for the same alloy the two bases can differ by tens of degrees, as the 904L and S32707 case studies made explicit.

Third, the pitting transition that defines the CPT is intrinsically nonlinear, because near the threshold individual passive-film rupture events cease to be independent and begin to interact through shared local chemistry. This coupling is exactly what the bispectrum is built to detect: as the CPT is approached, discrete peaks emerge in the bispectrum magnitude surface and the bispectral descriptors rise, while the wavelet energy migrates from fine to coarse crystals. The close agreement between the electrochemical-noise CPT of S32707 and its potentiostatic and impedance values reported by Xu et al. (2018) empirically anchors this picture, and the higher-order results of Darowicki and Zieliński (2008) and the wavelet results of Suresh and Kamachi Mudali (2014) supply direct support for the individual mechanisms.

Fourth, these observations point to an integrated acquisition-to-prediction methodology in which fused higher-order, wavelet, spectral and statistical descriptors are mapped—by physically motivated thresholds or by calibrated data-driven models—onto a CPT estimate and an early warning of stable pitting. Because coupling appears as the metastable pit population organises, such a method offers the prospect of detecting the approach to the CPT earlier than criteria based on average current, and of doing so non-perturbatively and in the service electrolyte.

The outlook rests on closing three gaps. The community needs systematic bispectral studies of highly alloyed grades—904L, the super-duplex grades and hyper-duplex S32707—in seawater and brine, so that the relationship between bispectral onset and the standard CPT criterion is calibrated for the materials that matter for desalination. It needs standardisation of acquisition, conditioning and higher-order estimation so that results are comparable between laboratories. And it needs field validation of fused-feature models under the fouling, flow and biofilm conditions of real plant. If these are achieved, electrochemical noise interpreted through higher-order and time–frequency analysis could move the assessment of pitting resistance from an intermittent laboratory measurement toward a continuous, predictive element of corrosion management for stainless steels in the most aggressive chloride environments.

More broadly, this review illustrates a principle that extends beyond the specific case of the critical pitting temperature. Corrosion processes carry their mechanistic signatures in the statistics of the fluctuations they generate, and the richness of those signatures is accessible only to analysis that goes beyond first- and second-order measures. The mean current and the noise resistance report that a surface is active; the power spectrum reports how the activity is distributed in frequency; but only the higher-order and time–frequency descriptions reveal the organisation of the underlying events—whether they remain a random shower of independent transients or have begun the cooperative, coupled behaviour that precedes failure. For a threshold phenomenon like the CPT, such that the engineering question is whether a surface has crossed from benign to dangerous behaviour, this sensitivity to organisation is not a refinement but the essential point. As

acquisition hardware, computing power and machine learning tools continue to mature, the barrier to routine higher-order interpretation of corrosion signals is lowering and the notion of treating a corroding surface as a signal source to be decoded rather than merely a mass to be weighed after the fact seems to have made a leap from aspiration to reality. The pitting of stainless steels in seawater and brine, with its sharp, reproducible and economically relevant threshold, is the most promising place to start.

CONFLICT OF INTEREST

The authors declare that there is no conflict of interest.

ACKNOWLEDGMENET

The author would like to express his sincere gratitude to **Dr. Mohd Aarif** for his valuable contributions to the research, particularly his efforts in data analysis, data evaluation, and programming. His technical expertise, insightful input, and dedicated support have significantly contributed to the successful completion of this work. The authors deeply appreciate his time, cooperation, and professional assistance.

REFERENCES

[1] Aballe, A., Bethencourt, M., Botana, F. J., & Marcos, M. (1999). Using wavelet transform in the analysis of electrochemical noise data. *Electrochimica Acta,* 44(26), 4805–4816. https://doi.org/10.1016/S0013-4686(99)00222-4

[2] Aballe, A., Bethencourt, M., Botana, F. J., Marcos, M., & Sánchez-Amaya, J. M. (2001). Use of wavelets to study electrochemical noise transients. *Electrochimica Acta,* 46(15), 2353–2361. https://doi.org/10.1016/S0013-4686(01)00442-6

[3] Arnvig, P.-E., & Bisgard, A. D. (1996). Determining the potential independent critical pitting temperature (CPT) by a potentiostatic method using the Avesta Cell. In Corrosion/96 (Paper No. 437). *NACE International.*

[4] ASTM International. (2020a). Standard test methods for pitting and crevice corrosion resistance of stainless steels and related alloys by use of ferric chloride solution (ASTM G48-11(2020)e1). *ASTM International.*

[5] ASTM International. (2020b). Standard test method for electrochemical critical pitting temperature testing of stainless steels and related alloys (ASTM G150-18). *ASTM International.*

[6] Bertocci, U., Gabrielli, C., Huet, F., & Keddam, M. (1997). Noise resistance applied to corrosion measurements: I. Theoretical analysis. *Journal of the Electrochemical Society,* 144(1), 31–37. https://doi.org/10.1149/1.1837361

[7] Calabrese, L., Galeano, M., & Proverbio, E. (2023). Data mining of electrochemical noise signals for the identification of corrosion phenomena. *Corrosion and Materials Degradation,* 4(4), 659–679. https://doi.org/10.3390/cmd4040034

[8] Cardenas-Barrera, J. L., et al. (2024). Machine-learning approaches to the interpretation of electrochemical noise for corrosion monitoring. *Corrosion Reviews*, 42(2), 145–168.

[9] Chen, A., Cai, Z., & Wang, Y. (2019). Pitting corrosion behaviour of super duplex stainless steel in chloride environments. *Materials,* 12(9), 1512. https://doi.org/10.3390/ma12091512

[10] Collis, W. B., White, P. R., & Hammond, J. K. (1998). Higher-order spectra: The bispectrum and trispectrum. Mechanical Systems and Signal Processing, 12(3), 375–394. https://doi.org/10.1006/mssp.1997.0145

[11] Cottis, R. A. (2001). Interpretation of electrochemical noise data. *Corrosion,* 57(3), 265–285. https://doi.org/10.5006/1.3290350

[12] Darowicki, K., & Zieliński, A. (2008). Application of the bispectrum in the analysis of electrochemical noise generated during metastable pitting of stainless steel. *Journal of Solid State Electrochemistry*, 12(12), 1573–1581. https://doi.org/10.1007/s10008-008-0643-y

[13] Davis, J. R. (Ed.). (2000). Corrosion: Understanding the basics. *ASM International.*

[14] Frankel, G. S. (1998). Pitting corrosion of metals: A review of the critical factors. *Journal of the Electrochemical Society,* 145(6), 2186–2198. https://doi.org/10.1149/1.1838615

[15] Galvele, J. R. (1976). Transport processes and the mechanism of pitting of metals. *Journal of the Electrochemical Society*, 123(4), 464–474. https://doi.org/10.1149/1.2132857

[16] Homborg, A. M., Tinga, T., Zhang, X., van Westing, E. P. M., Oonincx, P. J., de Wit, J. H. W., & Mol, J. M. C. (2012). Time–frequency methods for trend removal in electrochemical noise data. *Electrochimica Acta*, 70, 199–209. https://doi.org/10.1016/j.electacta.2012.03.062

[17] Hou, Y., Aldrich, C., Lepkova, K., Machuca, L. L., & Kinsella, B. (2017). Monitoring of carbon steel corrosion by use of electrochemical noise and recurrence quantification analysis. *Electrochimica Acta*, 256, 337–347. https://doi.org/10.1016/j.electacta.2017.10.063

[18] Jian, W., Yunhe, Z., Yuanhang, Z., Wei, L., & Jianchun, F. (2026). Electrochemical noise analysis on corrosion behavior of nickel-based superalloy. *Journal of Materials Engineering and Performance*. Advance online publication. https://doi.org/10.1007/s11665-026-13545-3

[19] Laycock, N. J., & Newman, R. C. (1997). Localised dissolution kinetics, salt films and pitting potentials. *Corrosion Science,* 39(10–11), 1771–1790. https://doi.org/10.1016/S0010-938X(97)00049-8

[20] Macdonald, D. D. (2011). The history of the Point Defect Model for the passive state: A brief review of film growth aspects. *Electrochimica Acta,* 56(4), 1761–1772. https://doi.org/10.1016/j.electacta.2010.11.005

[21] Marcus, P. (Ed.). (2011). Corrosion mechanisms in theory and practice (3rd ed.). *CRC Press*.

[22] Maurice, V., & Marcus, P. (2017). Current developments of nanoscale insight into corrosion protection by passive oxide films. Current Opinion in Solid State and Materials Science, 22(4), 156–167. https://doi.org/10.1016/j.cossms.2018.05.004

[23] Nakhaie, D., & Asselin, E. (2026a). Reproducibility of critical crevice temperature (CCT) measurements for two duplex stainless steels. *Journal of The Electrochemical Society*, 173(6), 061503. https://doi.org/10.1149/1945-7111/ae534b

[24] Nakhaie, D., & Asselin, E. (2026b). Revisiting the effect of sulfate in mixed chloride–sulfate media: Critical temperatures, potentials, and pit chemistry of 2205 duplex stainless steel. *Journal of The Electrochemical Society*, 173(11), 111504. https://doi.org/10.1149/1945-7111/ae720b

[25] Newman, R. C. (2001). W. R. Whitney Award Lecture: Understanding the corrosion of stainless steel. *Corrosion*, 57(12), 1030–1041. https://doi.org/10.5006/1.3281676

[26] Nikias, C. L., & Petropulu, A. P. (1993). Higher-order spectra analysis: A nonlinear signal processing framework. *Prentice Hall.*

[27] Nilsson, J.-O. (1992). Super duplex stainless steels. *Materials Science and Technology*, 8(8), 685–700. https://doi.org/10.1179/mst.1992.8.8.685

[28] Pistorius, P. C., & Burstein, G. T. (1992). Metastable pitting corrosion of stainless steel and the transition to stability. Philosophical Transactions of the Royal Society A, 341(1662), 531–559. https://doi.org/10.1098/rsta.1992.0114

[29] Pujar, M. G., Anita, T., Shaikh, H., Dayal, R. K., & Khatak, H. S. (2011). Analysis of electrochemical noise data using power spectral density and wavelet transform for pitting corrosion of type 304 stainless steel. *International Journal of Electrochemical Science*, 6(4), 1077–1095.

[30] Ryan, M. P., Williams, D. E., Chater, R. J., Hutton, B. M., & McPhail, D. S. (2002). Why stainless steel corrodes. *Nature*, 415(6873), 770–774. https://doi.org/10.1038/415770a

[31] Salinas-Bravo, V. M., & Newman, R. C. (1994). An alternative method to determine the critical pitting temperature of stainless steels in ferric chloride solution. *Corrosion Science*, 36(1), 67–77. https://doi.org/10.1016/0010-938X(94)90109-0

[32] Sedriks, A. J. (1996). Corrosion of stainless steels (2nd ed.). Wiley-Interscience.

[33] Shahidi, M., Hosseini, S. M. A., & Jafari, A. H. (2011). Comparison between ED and SDPS plots as the results of wavelet transform for analyzing electrochemical noise data. *Electrochimica Acta*, 56(24), 9986–9997. https://doi.org/10.1016/j.electacta.2011.08.093

[34] Suresh, G., & Kamachi Mudali, U. (2014). Electrochemical noise analysis of pitting corrosion of type 304L stainless steel. *Corrosion,* 70(3), 283–293. https://doi.org/10.5006/1003

[35] Szklarska-Smialowska, Z. (1986). Pitting corrosion of metals. National Association of Corrosion Engineers.

[36] Sánchez-Amaya, J. M., Cottis, R. A., & Botana, F. J. (2005). Shot noise and statistical parameters for the estimation of corrosion mechanisms. *Corrosion Science*, 47(12), 3280–3299. https://doi.org/10.1016/j.corsci.2005.05.047

[37] Tan, Y.-J., Bailey, S., & Kinsella, B. (1996). The monitoring of the formation and destruction of corrosion inhibitor films using electrochemical noise analysis. *Corrosion Science*, 38(10), 1681–1695. https://doi.org/10.1016/S0010-938X(96)00061-3

[38] Upadhyay, N., Shankar, A. R., Singh, S. S., & Anandkumar, B. (2022). Electrochemical noise and wavelet analysis of the effect of nitrogen on the pitting corrosion of stainless steel. *Corrosion Engineering, Science and Technology*, 57(7), 611–622. https://doi.org/10.1080/1478422X.2022.2096323

[39] Xu, X.-q., Zhao, M., Feng, Y.-r., Li, F.-g., & Zhang, X. (2018). A comparative study of critical pitting temperature (CPT) of super duplex stainless steel S32707 in NaCl solution. *International Journal of Electrochemical Science*, 13(5), 4298–4310. https://doi.org/10.20964/2018.05.13